Title: **Arctic Sea Ice Parameters from AMSR-E Data using Two Techniques, and Comparisons with Sea Ice from SSM/I**

Authors: Josefino C. Comiso and Claire L. Parkinson
NASA Goddard Space Flight Center, Greenbelt, MD

Journal: **Journal of** Geophysical Research - Special section on "Large Scale Characteristics of the Sea Ice Cover from AMSR-E and other Satellites"

ABSTRACT: We use two algorithms to process AMSR-E data in order to determine algorithm dependence, if any, on the estimates of sea ice concentration, ice extent and area, and trends and to evaluate how AMSR-E data compare with historical SSM/I data. The monthly ice concentrations derived from the two algorithms from AMSR-E data (the AMSR-E Bootstrap Algorithm, or ABA, and the enhanced NASA Team algorithm, or NT2) differ on average by about 1 to 3%, with data from the consolidated ice region being generally comparable for ABA and NT2 retrievals while data in the marginal ice zones and thin ice regions show higher values when the NT2 algorithm is used. The ice extents and areas derived separately from AMSR-E using these two algorithms are, however, in good agreement, with the differences (ABA-NT2) being about 6.6 x 10^4 km^2 on average for ice extents and -6.6 x 10^4 km^2 for ice area which are small compared to mean seasonal values of 10.5 x 10^6 and 9.8 x 10^6 for ice extent and area, respectively. Likewise, extents and areas derived from the same algorithm but from AMSR-E and SSM/I data are consistent but differ by about -24.4 x 10^4 km^2 and -13.9 x 10^4 km^2, respectively. The discrepancies are larger with the estimates of extents than area mainly because of differences in channel selection and sensor resolutions. Trends in extent during the AMSR-E era were also estimated and results from all three data sets are shown to be in good agreement (within errors).

Popular Summary: The Aqua AMSR-E sensor provides the opportunity to observe the Arctic sea ice cover at a higher resolution and greater spectral range than previously possible and hence an improved accuracy in the characterization of the sea ice cover. The availability of the data is timely in light of rapid changes being observed in parts of the polar regions in recent years and the requirements of more accurate observations. We use ice concentrations derived from two AMSR-E algorithms to assess how consistently the ice cover can be characterized and how estimates of the Arctic sea ice extent and area as well as their trends would be affected by the use of different techniques. Such comparisons are especially important since the extent and area provide the means to assess the state of the sea ice cover and quantify impacts of Arctic warming that may be related to increasing anthropogenic greenhouse gases in the atmosphere. It is also essential to know to what extent such estimates can be algorithm dependent. The monthly ice concentrations derived from AMSR-E data using the two algorithms differ on average by about 1-3%, with data from near the ice edge generally higher when the NT2 algorithm is used. The standard deviations of the differences are also very small, being ±1.0, ±1.13, ±1.13, and ±1.0 % in summer, autumn, winter and spring, respectively. Slight adjustment in the tie-points for ice and water could make the difference even smaller. It is encouraging to get very good consistency in the extents and areas of the sea ice cover as derived from AMSR-E data using two algorithms that are formulated quite differently and make use of different sets of AMSR-E channels, as it is highly desired that the characterization of the ice cover, including its ice extent and area, would be independent of technique, allowing for confidence in the results. Likewise, it is satisfying to get good agreement of extents and areas derived when data from AMSR-E are compared with those from SSM/I using the same algorithm. There are slight biases associated with the

differences in the resolution of the different sensors in the estimates of ice extents but this is basically negligible in estimates of ice area. A bias, if uncorrected would cause significant errors in trend estimates when combining AMSR-E with historical data. Fortunately, a long overlap of AMSR-E and SSM/I data exists and this will provide the means to remove biases before incorporating the more accurate AMSR-E data in the time series.

Significant Findings: We use ice concentrations derived from two AMSR-E algorithms to assess how consistently the ice cover can be characterized and how estimates of the Arctic sea ice extent and area as well as their trends would be affected by the use of different techniques. The monthly ice concentrations derived from AMSR-E data using the two algorithms differ on average by about 1-3%, with data from near the ice edge generally higher when the NT2 algorithm is used. The standard deviations of the differences are also very small, being ±1.0, ±1.13, ±1.13, and ±1.0 % in summer, autumn, winter and spring, respectively. Slight adjustment in the tie-points for ice and water could make the difference even smaller. It is encouraging to get very good consistency in the extents and areas of the sea ice cover as derived from AMSR-E data using two algorithms that are formulated quite differently and make use of different sets of AMSR-E channels, as it is highly desired that the characterization of the ice cover, including its ice extent and area, would be independent of technique, allowing for confidence in the results. Likewise, it is satisfying to get good agreement of extents and areas derived when data from AMSR-E are compared with those from SSM/I using the same algorithm. There are slight biases associated with the differences in the resolution of the different sensors in the estimates of ice extents but this is basically negligible in estimates of ice area. A bias, if uncorrected would cause significant errors in trend estimates when combining AMSR-E with historical data. Fortunately, a long overlap of AMSR-E and SSM/I data exists and this will provide the means to remove biases before incorporating the more accurate AMSR-E data in the time series. Overall, the merit of each algorithm depends on application but it is encouraging to know that they produce approximately the same trends in ice extent and area and that the differences in ice concentration values are well within the 5-10% estimated errors in the ice concentration determinations.

Arctic Sea Ice Parameters from AMSR-E Data using Two Techniques, and Comparisons with Sea Ice from SSM/I

Josefino C. Comiso and Claire L. Parkinson
NASA Goddard Space Flight Center, Greenbelt, MD

Submitted the Journal of Geophysical Research on 30 March 2007
Special section on "Large Scale Characteristics of the Sea Ice Cover from AMSR-E and other Satellites"

Short Title: Arctic Sea Ice from AMSR-E

Keywords: sea ice, Arctic ocean, cryosphere, climate change, remote sensing

ABSTRACT

We use two algorithms to process AMSR-E data in order to determine algorithm dependence, if any, on the estimates of sea ice concentration, ice extent and area, and trends and to evaluate how AMSR-E data compare with historical SSM/I data. The monthly ice concentrations derived from the two algorithms from AMSR-E data (the AMSR-E Bootstrap Algorithm, or ABA, and the enhanced NASA Team algorithm, or NT2) differ on average by about 1 to 3%, with data from the consolidated ice region being generally comparable for ABA and NT2 retrievals while data in the marginal ice zones and thin ice regions show higher values when the NT2 algorithm is used. The ice extents and areas derived separately from AMSR-E using these two algorithms are, however, in good agreement, with the differences (ABA-NT2) being about 6.6 x 10^4 km^2 on average for ice extents and -6.6 x 10^4 km^2 for ice area which are small compared to mean seasonal values of 10.5 x 10^6 and 9.8 x 10^6 for ice extent and area, respectively. Likewise, extents and areas derived from the same algorithm but from AMSR-E and SSM/I data are consistent but differ by about -24.4 x 10^4 km^2 and -13.9 x 10^4 km^2, respectively. The discrepancies are larger with the estimates of extents than area mainly because of differences in channel selection and sensor resolutions. Trends in extent during the AMSR-E era were also estimated and results from all three data sets are shown to be in good agreement (within errors).

1. Introduction

The extent and area of the sea ice cover are key parameters needed to assess the state of the cryosphere and monitor the Earth's climate system. Prior to satellites, knowledge about these parameters was scant and inferred from limited human observations in different parts of the Arctic (Walsh and Johnson, 1979). With the pan-Arctic ice cover so vast and dynamic, it was not until the advent of satellite remote sensing that quantitative assessments of the extent and area of sea ice for the entire Northern Hemisphere could be made. Among the first such estimates were those derived from data provided by the Electrically Scanning Microwave Radiometer (ESMR), which is a single channel system (at 19 GHz) launched in December 1972 aboard NASA's Nimbus-5 satellite (Parkinson et al., 1987). These data were suitable for estimates of the extent of sea ice covered areas because of the large contrast in emissivity between sea ice and liquid water. However, there were ambiguities in the estimates of sea ice concentration primarily because of large differences in the emissivity of seasonal first year (FY) ice and multiyear (MY) ice (Vant et al., 1976; Comiso, 1983) and the difficulty of discriminating the latter from mixtures of open water and first year ice. The launch of the Scanning Multichannel Microwave Radiometer (SMMR) on board NASA's Nimbus-7 satellite in October 1978 made it possible to overcome the problem because of its multifrequency and multipolarization capability, which enabled the accounting of spatial changes in the emissivity of the surface. SMMR was followed by a similar instrument called the Special Sensor Microwave Imager (SSM/I), first launched in July 1989 on the F8 satellite in the Defense Meteorological Satellite Program (DMSP) series. Additional SSM/I instruments have been launched on the F11 and F13 satellites. The SSM/I sensors are considered 'operational' rather than 'research' instruments and are launched in succession to ensure that as one degrades or fails to operate, it is replaced by another. The combination of the SMMR and SSM/I instruments has enabled a near-continuous time series of consistent data on sea ice to be generated from November 1978 to the present.

A new satellite microwave sensor from Japan called the Advanced Microwave Scanning Radiometer for the Earth Observing System (AMSR-E) was launched on board NASA's Aqua satellite in May 2002 with capabilities that exceed those of SMMR and SSM/I because of a larger antenna (yielding higher spatial resolution) and wider spectral range. The new AMSR-E data indeed provide superior coverage of the sea ice cover and will likely be the baseline for studies of the ice cover in the years to come (Comiso et al., 2003; Markus and Cavalieri, 2000). However, its capabilities need to be evaluated and validated and also should be compared quantitatively with those of SSM/I and SMMR data. The derived values have been shown to be consistent with those from Aqua's Moderate Resolution Imaging Spectroradiometer (MODIS), which provides concurrent high resolution visible and infrared data. The goal is to be able to be able to assess the accuracy in the data that are currently used for monitoring the changes in the sea ice cover. While rapid declines have been reported in the Arctic perennial ice cover (Comiso, 2002; Comiso and Parkinson, 2004) the trends for the entire Northern Hemisphere have been more modest at about 3% per decade (e.g., Bjorgo et al., 1997; Cavalieri et al., 1997; Parkinson et al., 1999). Accurate data are also needed to validate modeling studies that have projected declines in the ice cover due to global warming caused in part by increasing greenhouse gases in the atmosphere (Holland and Bitz, 2003). In this study, we assess the general characteristics of the Arctic sea ice cover as inferred from two sea ice algorithms. In particular we compare sea ice concentrations derived from these algorithms and assess quantitatively how the differences are reflected in estimates of sea ice extents, ice areas and trends. This enables us to examine whether the characterization of the sea ice cover is algorithm-dependent and if so, why. Also, we compare AMSR-E data with SSM/I data, to assess how the new data set can be used in conjunction with historical data to improve our characterization of the state of the sea ice cover. A companion paper (Parkinson and Comiso, 2007) examines the Antarctic sea ice cover with the same two algorithms and instruments.

2. Ice Algorithms, Data Reduction, Masks, and Sensitivity Studies

The AMSR-E sensor has a total of 14 channels and measures microwave radiation from the Earth's surface at 7 frequencies (from 6.9 to 89.0 GHz) and at both vertical and horizontal polarizations. It is a conically scanning system with a swath-width of about 1445 km and obtains data from practically the entire Arctic in less than a day, with an incidence angle fixed at about 55°. The integrated field-of-view of the sensor is 73.0 by 43.1 km at 6.9 GHz, improving with frequency to about 6.0 by 4.9 km at 89.0 GHz. The key AMSR-E frequencies that have been used for sea ice algorithms are 18.7 GHz and 36.5 GHz, with estimated ground resolution of about 26.2 by 16.5 km and 13.7 by 10.3 km, respectively. For comparison, the corresponding ground resolutions for the SMMR and SSM/I data at approximately the same frequencies are 54 by 35 km and 28 by 18 km for SMMR and 70 by 40 km and 38 by 30 km for SSM/I. The improvement in the resolution of AMSR-E data over those of historical data is therefore quite considerable. The resolution of AMSR-E at 89 GHz as indicated above is even better and could be utilized for many mesoscale studies; the 89 GHz resolution approaches that of the Advanced Very High Resolution Radiometer (AVHRR) Global Area Coverage (GAC) data, which have been used for detecting leads within the ice pack during cloud free conditions. However, the discrepancy of AMSR-E resolution with those of historical data requires special attention in order to obtain sea ice results consistent with the historical record. The 89 GHz data are promising in vew of their spatial resoltuion but are difficult because of high sensitivity to atmospheric conditions and snow cover.

Orbital AMSR-E data have been mapped to a polar-stereographic grid at resolutions of about 12.5 by 12.5 km and 25 by 25.0 km using the 'drop-in-a-bucket technique', meaning that the near instantaneous brightness temperature observed by the sensor at a certain latitude and longitude point is assigned to an (i,j) grid element that encloses this geographical coordinate. To make the area of the polar grid nearly uniform, the mapping plane cuts the Earth's surface at 70 degrees latitude. This gridding system has been used for generating daily averages of day and night data as well as daily sea ice data from AMSR-E and is consistent with the gridding system used with the SSM/I and SMMR sea ice data.

Several sea ice concentration algorithms have been developed for multichannel passive microwave data over the years (e.g., Cavalieri et al., 1984, Swift et al., 1985; Svenson et al., 1986; Comiso, 1986; Steffen et al., 1992). The techniques have been refined and adapted for AMSR-E data, and for this study, we use two algorithms called the AMSR-E Bootstrap Algorithm (ABA) and the NASA Team (version 2) Algorithm (NT2), as discussed in Comiso et al. (2003).

With a single channel, ice concentration (C) can be derived from satellite measurements of brightness temperature, T_B, using the following mixing equation that expresses the measurements as the sum of the two components of interest being either sea ice (I) or open water (W):

$$T_B = C\,T_I + (1-C)\,T_W \qquad (1)$$

where T_I and T_W are the brightness temperatures of 100% ice and 100% open water, respectively. T_I and T_W are usually called the 'tie points' for 100% and 0% ice cover, respectively. Equation (1) looks simple, but the estimate of C is complicated by the variability of the brightness temperature over ice covered and open water areas; hence the need for a more sophisticated algorithm, involving more than one channel. In the microwave region, following the Rayleigh-Jeans formulation, the brightness temperature can be estimated closely by the product of the emissivity and the temperature of the emitting surface. Although the emissivity of open water within the ice pack (which is usually under calm conditions) is reasonably stable, the emissivity of sea ice changes considerably depending on stage of ice growth, snow cover, thickness, and salinity. The physical temperature of the emitting layer, which is usually that of the snow/ice interface, is also variable although the changes are moderate (about 2.5 ^{o}C standard deviation) after the sea ice has acquired a snow cover.

The ABA technique identifies the tie-points in equation (1) by making use of results from a cluster and regression analysis of sets of AMSR-E channels. The primary data sets used are those from 18.7 GHz at vertical polarization and 36.5 GHz at both vertical and horizontal polarizations; these have reasonable resolution and predictable emissivities over ice covered areas, as discussed in Comiso et al. (2003). The NT2 technique uses the same sets of channels formulated as gradient and polarization ratios, as in the original NT technique, and in addition makes use of the 89 GHz channel at vertical polarization to minimize errors associated with snow layering and other characteristics that affect one polarization channel more than the other (Markus and Cavalieri, 2000; Comiso et al., 2003). To compensate for the high sensitivity of the 89 GHz channel to snow and atmospheric effects, an atmospheric radiative transfer program is used. A challenge for the latter is how effectively a radiative transfer program can keep track of the surface emissivity at this frequency, which is unpredictably variable over sea ice covered regions. Previous comparative analysis of ice concentrations using the bootstrap and the NASA team algorithms showed large discrepancies (Comiso et al., 1997). The current study shows that the ice concentrations from the ABA and NT2 algorithms still have some discrepancies, but these are much smaller than those identified from the earlier versions of the algorithms (i.e., in Comiso et al., 1997).

A key concern with the use of data from different frequencies is the markedly different resolutions for the different frequency channels. The footprint of the 18.7, 36.5 and 89 GHz channels are 432.3, 141.1, and 29.4 km^2, respectively. Thus, the instantaneous information that the AMSR-E 18.7 GHz sensor provides comes from an area about 15 times larger than that from the 89 GHz channel. The compromise solution is to use a grid resolution intermediate to the resolutions of 18.7 and 89 GHz and basically to degrade the resolution of the 89 GHz data. Two grid sizes are currently being used for mapping the AMSR-E sea ice data: 12.5 by 12.5 km (156.2 km^2) and 25 by 25 km (625 km^2). The use of the 12.5 by 12.5 km grid is justified in part by the fact that the distance between successive swaths along the satellite orbit is 10 km. Experience has shown that we get almost identical results from the 12.5 km gridded data and the 25 km data when the former is degraded to the resolution of the latter. For studies that require optimum resolution, the 89 GHz TB data have been mapped to a 6.25 by 6.25 km grid and ice concentration is derived using just the 89 GHz channels, e.g., using the Bootstrap technique adjusted for the 89 GHz channels. Again, such data should be used with caution, in view of the sensitivity to atmospheric conditions and snow cover.

Another source of concern is the information content of derived data from the different frequencies and polarization. For example, the contrast in emissivity between water and first year ice is higher with lower frequency data. Also, the penetration depth through the snow and ice is frequency dependent, with the radiation at lower frequencies (i.e., longer wavelengths) penetrating much deeper than the radiation at higher frequencies. Thus, the radiation detected by the radiometers at different frequencies comes from different layers of the ice cover and, in some cases, even different types of layers. For example, the observed brightness temperature at 18.7 GHz from the seasonal ice cover usually originates from the snow/ice interface since snow is relatively transparent to radiation at this frequency, whereas at 89 GHz, the brightness temperature observed may come primarily from the snow cover. Therefore, although algorithms incorporating different channels are designed to produce the same ice concentration values, differences associated with the choice of channels can lead to somewhat different results. The discrepancies in the origin of the signals are in part taken into account through the use of scatter plots of sets of frequency (and polarization) channels that enable identification of signatures (i.e., tie points) of consolidated sea ice from the different frequency and polarization measurements. The choice of tie points is technique-dependent (Comiso et al., 2003); and a change in tie points results in different estimates for ice concentrations. The latter allows tie points to be used as 'tuning' parameters for the ice-concentration algorithms.

An important consideration is that the multichannel signatures of different surfaces on land can be quite similar to those over sea ice. For simplicity, a land mask derived using published land boundaries and high resolution satellite data, is used. Figure 1 provides a location map of land areas including small islands in the high latitude regions of the Northern Hemisphere. The figure also shows typical sea ice distributions during annual maximum and minimum ice coverage, as derived from historical satellite data. In winter, sea ice covers practically the entire Arctic basin and extends well out into many of the surrounding seas and bays. We know that the continental boundaries (generally delineated as extending to the edge of ice shelves where they exist) are actually not constant with time, especially in areas covered by ice shelves and glaciers, which are constantly changing due to melt, ice calving and surging. Unfortunately, a monitoring technique that keeps track of all continental boundary changes on a day-to-day basis currently does not exist, hence hindering the production of a land mask appropriate for each day (or even just each month) of data. With the observation of large calving events in recent years, such capabilities would be desirable. However, in this study, a fixed land mask is used for all data processed, with the same, constant land mask used for the ABA and NT2 algorithms. A notable advantage of the constant land mask is that it facilitates comparisons and determination of trends.

A complication recognized since ice concentrations were first calculated from satellite data in the 1970s is that ocean data adjacent to the land-ocean boundaries are contaminated by signals from land. At these boundaries, there are data elements (pixels) that contain mixtures of land and ocean areas. In addition, radiometer side-lobe effects make the measurements at the ice edge different when the satellite crosses the boundary from land to ocean as opposed to ocean to land. Also, having footprints for some channels that are larger than the size of the grid causes a smearing effect. As a result, the algorithms yield non-zero ice concentrations near the land-ocean boundary (a few pixels beyond the boundary) even in regions that are unquestionably ice-free, like along the coast of Spain. These faulty indications of ice would cause large errors in the estimates of ice extent and ice area if not corrected. To overcome this problem, the NT2 algorithm uses monthly sea surface temperature fields to establish a threshold for where sea ice is not allowed, and the Bootstrap algorithm uses an enhanced version of a technique described in Cho (1996), with residual clearly extraneous derived ice being removed manually. Neither technique is perfect but both considerably reduce the land contamination effect.

Extraneous non-zero ice concentrations at different but significant levels are also derived by the algorithms in the open ocean regions. This comes about because the microwave signatures of open ocean during adverse weather conditions with large waves, foam, and rain, can be similar to the signatures of ice covered ocean. For the Bootstrap algorithm, general filtering technique makes use of the unique patterns produced by data points belonging to ocean regions in scatter plots of different sets of AMSR-E channels as shown in Figure 2. Data from ice free ocean are represented in Figure 2 by the blue dots and can be classified as ice free areas by setting thresholds that separate them from ice covered areas. Ambiguities are not easy to eliminate since at the cut-off point near the ice edge, it is difficult to obtain a consistent threshold value in units of ice concentration, due to the different emissivities of different sea ice types. Also, waves tend to cause ice rafting and flooding over the ice, both of which cause the ice emissivity to be even less well-defined. The ocean mask employed by the Bootstrap Algorithm for AMSR-E data is illustrated in Figure 2a and 2b, using the sets of 19, 22, and 37 GHz channels as shown. The corresponding mask used by NT2 for AMSR-E data is shown in 2c. In the scatter plots in Figures 2a and 2b, the data points that are clustered together from the point labeled O to W correspond to data in the open ocean. These data points (in blue) are easier to discriminate from the ice covered data points (in black) in Figure 2a, which makes use of the 22 GHz channel (vertical polarization), than in Figure 2b. The plot in Figure 2a is thus used as the primary mask for the ABA data set, and Figure 2b is used primarily to remove residuals. A slanted line which corresponds to ice concentrations of about 10% is drawn in the scatter plots and data below this line are considered ice free (or less than 10% ice concentration). Such a threshold is used since below 10% ice concentration, it is difficult to discriminate ice covered data from data without ice cover. In fact, in our ice concentration images we use a 12% threshold, and in our ice extent calculations we use a 15% threshold. The NT2 data set makes use of a similar technique but using gradient and polarization ratios in the scatter plot as illustrated in Figure 3a and 3b for the basic ocean mask for SSM/I and AMSR-E, respectively, while Figures 3c and 3d serve as a supplement to mask out residuals as discussed in Markus and Cavalieri (2000).

Some of the differences, especially in ice extent observed in this study, are associated with the differences in the data screened by the two techniques as either open water areas or ice covered areas. There are also differences in the "open ocean tie-points" which are expected to represent the microwave signatures of open water within the ice pack. The clusters in Figure 2 and 3 provide the means to evaluate what this signature is; on the average, open water within the pack represents stable surface conditions that normally correspond to low brightness temperature values (i.e., close to the point O in Figures 2 and 3). Differences in tie point location affect the estimates of ice concentration, especially at low concentration values. To facilitate interpretation of the results when doing comparative analysis in this study, we make the masked areas in the open ocean and the land/ocean boundaries (especially in regions away from the ice pack) in the two data sets as consistent as possible.

3. Ice Concentration Maps, Extents, and Ice Areas

3.1 Ice Concentrations

Color-coded monthly ice concentration maps derived from AMSR-E data using the ABA and NT2 algorithms for four different years in summer (August), autumn (November), winter (February), and spring (May) are presented in Figures 4, 5, 6 and 7, respectively, to illustrate the differences in ice concentrations calculated using the two different algorithms. Despite differences in the technique and sets of channels used, the monthly sea ice concentration maps from the two algorithms are fortunately quite similar, as both are attempting to depict the same parameter. In the sets of images, both algorithms yield very high concentrations within the ice pack, reflecting fully or near fully consolidated ice cover in the inner zone during the various periods, and good consistency in the location of the ice edges. There are subtle differences of usually less than 10 % ice concentration and these are quantified better with the difference maps shown in the last column of Figures 3-6. In the inner pack, the ABA and NT2 concentrations are generally comparable, although with some areas of significant differences, while in the marginal ice zones, the ABA concentrations are usually less, especially in the non-summer months.

The differences in ice concentration are likely associated with use of different sets of channels in the two algorithms, as described in section 2. Perhaps most importantly, NT2 makes use of the 89 GHz channel in combination with the 19 and 37 GHz channels while ABA makes use of the 19 and 37 GHz channels only. The emissivity of sea ice generally increases with thickness up to a relatively stable maximum value for first year (or seasonal) ice. This maximum value occurs at a certain thickness but the specific thickness varies with frequency (or wavelength of the radiation). This is because the penetration depth of the radiation varies inversely with frequency and therefore the maximum emissivity is reached when the ice is considerably thinner at 89 GHz than at 19 or 37 GHz. The use of a tie point that utilizes the 89 GHz data would therefore provide generally higher ice concentration values in the generally thin ice areas in the seasonal regions that those that use the lower frequencies only. However, the emissivity of ice at 89 GHz is not as stable over consolidated ice, and this may in part explain why the ice concentrations inside the pack in the Arctic basin are often higher for the ABA than for the NT2. Among the few exceptions is the area near the North Pole in the February 2004 images (i.e., negative values in the difference maps); this might have been an area of divergence at the time and hence might have had considerable thin ice. The emissivity for seasonal ice changes with thickness and granularity of the snow cover, but the multichannel algorithms take this into account, at least in part. The emissivity of ice may also be affected by changes in brine distribution and overall ice salinity during early stages of growth.

During late spring and summer, the surface of the ice cover transforms first from a generally dry surface to a slightly wet surface and then to slush, with some areas covered by meltponds (i.e., standing water on the surface of the ice floes). The emissivity of the surface during the early melt period is very high, almost similar to that of a blackbody, because at this stage, the presence of liquid makes the absorption coefficient of the snow very high. Further melt, however, transforms the material into slush, or almost melted snow, the emissivity of which is relatively low and close to that of water. As the snow continues to melt, the variability of the topography of the ice surface leads to the formation of melt ponds the signature of which is similar to that of open water (e.g., Comiso and Kwok, 1996; Markus and Dokken, 2002). Thus the uncertainties in the estimates for ice concentration are greatest in summer, explaining in part why it is the August images (Figure 4) that are most different for the two algorithms. In the inner pack in August, data from the ABA overall show higher values, while near the ice edge, data from NT2 are generally higher. In autumn (Figure 5) the two sets of images are very similar but there some areas of reduced ice concentrations in one but not in the other within the ice pack. Again, the marginal ice zones are locations of discrepancies. In the mid-winter (Figure 6) the agreement is also good, with the difference maps showing mainly near-0 values in the inner pack and negative biases in the marginal ice zones. In spring (Figure 7), the agreement is again very good. It is interesting that in some seasonal areas like Hudson Bay, the differences were negative in 2003 and 2005 but primarily positive or near 0 in 2004 and 2006. This may be associated with the same melt phenomenon that occurs in summer.

To assess the differences of the ABA and NT2 concentrations more quantitatively, histograms of the difference maps for the different years and seasons are presented in Figure 8. The histograms are highly peaked at a value near 0, indicating that the concentrations basically agree, although asymmetries are apparent, with a bias toward negative values in autumn, winter, and spring but toward positive values in summer, all in line with the images of Figures 4-7. The year-to-year variations for each of the four seasons are quite small. The peak value of the histograms varies with season, as expected, depicting the large seasonality of the sea ice cover. Gaussian fits were applied on each histogram, and the average standard deviation of the peaks in each of the four years were found to be, ±1.0, ±1.1, ±1.1, and ±1.0 % for the summer, autumn, winter and spring, respectively.

3.2 Ice Extents and Areas

To quantitatively assess the large scale characteristics and state of the sea ice cover and its variability, we estimate the ice extents and ice area. Ice extent is the sum of the area of all data elements in the study region that have ice concentrations of 15% and higher. The 15% threshold is used because of aforementioned uncertainties in ice concentration values near the ice edges and thin ice regions and the possibility of including many faulty data points if the threshold is set at a lower level. This is also the threshold for ice extent used in many previous studies (e.g., Parkinson et al., 1987, 1999). Ice area is the integrated sum of the area covered by sea ice (i.e., sum of the products of the area of the pixel and the ice concentration in the pixel). In general, the ice extent provides the means to estimate the total area directly impacted by sea ice. On the other hand, the ice area provides actual ice coverage and the data needed in combination with average ice thickness to estimate total volume and mass of the ice cover. Both parameters are needed to assess how the state of the cryosphere as reflected by the sea ice cover is changing.

Comparative analysis of ice concentration and extents requires considerations regarding how well the ice edges are represented by the different data sets. Plots of typical ice concentrations from a daily average map (specifically, one from 19 February 2006) along a transect from open water regions into the ice pack illustrates how the ice edges are represented by AMSR-E ice concentration data as derived from the ABA and NT2 algorithms (Figure 9). The data plotted are along a longitudinal line at 35° E and 45 ° E in the Barents Sea. The ice concentration data using ABA and NT2 both rise above 0 % at approximately 76.4°N, with the NT2 data rising slightly more rapidly than the ABA data. Also, the ice concentrations for NT2 rise to near 100% in about 100 km and then remain near 100%, while the ABA ice concentrations remain below 100% for another 50 km, which suggests that the ABA is perhaps more sensitive to some features of the outer zone of the ice cover than the NT2. In this specific transect, the edge of the ice, as defined by 15% ice concentration in the calculation of ice extent, comes sooner (from open water into the pack) by about 5 km in the NT2 calculations than the ABA calculations. In much of the region near the ice edge, likely the ice cover consists mainly of pancake ice and is relatively mobile because of wind and wave action, the effect of which decreases, overall, from the ice edge into the pack. The latitude at which the ABA and NT2 ice concentration data both converge to about 100 % is likely where the ice cover becomes consolidated and is no longer much affected by ocean swell. Similar phenomenon is apparent at 45°E, but this time the 15% ice edge occurs at about the same time and the values converge to 100% ice cover sooner into the pack. The space between pancakes is often covered by grease ice during autumn and winter; and the grease ice becomes the glue that transforms the region into consolidated ice. In contrast, the space between ice floes during spring and summer is often not covered by grease ice or other ice forms. As explained earlier, the average concentration in primarily new ice regions is expected to be higher with the NT2 than with the ABA, since the former saturates faster with thickness because of the use of the 89 GHz channel. In an area with considerable grease ice, NT2 likely captures the grease ice more accurately and obtains more accurate ice concentration values, while the ABA might provide more information regarding areas of divergence and the character of the marginal ice zone.

Daily ice extent and area of the sea ice cover over an annual cycle (2005) in the Northern Hemisphere are presented in Figure 10 to illustrate how values derived from the NT2 and ABA algorithms differ. For comparison, in addition to the NT2 and ABA AMSR-E values, corresponding values from the SSM/I data using the Bootstrap algorithm (SBA) are included in Figure 10 as well. The latter provide the means to evaluate how data derived from different sensors but the same algorithm compare. Daily data are used to illustrate changes in these parameters at a smaller time scale than in the monthly averages. Although large daily changes are known to occur at the ice edge, the net changes in extent and area are modest in part because negative changes (or retreat) in one place are often compensated by positive changes (or advance) in other places. The plots indicate a generally good consistency of extents and areas from the three data sets, although with the SBA data showing consistently higher values for extent than the other two. As explained earlier, higher values for extent can be caused by lower resolution, which is the case for SSM/I data. The differences in the ABA and NT2 extents are most pronounced during the summer, as reflected also in the ice concentration maps (Figures 3-6) while the areas are mainly consistent, especially during the autumn.

Monthly averages of the ABA and NT2 ice extents and ice areas during the 2002-2006 period (when AMSR-E data are available) provide the means to assess monthly and interannual changes in the ice cover (Figures 11a and 11b). The variability in the extent and in the area are in part associated with the variability in the ice concentrations, the monthly averages of which are also shown in Figure 11c. The year-to-year variability in the ice extents during the AMSR-E era are consistently represented by ABA and NT2 data, with the summer season showing the largest difference (Figure 11), as in Figure 10. The ice areas have better consistency in the summer but show slight discrepancies in the winter period, with the NT2 values having slightly higher values. These wintertime discrepancies are reflected by the higher average ice concentrations derived from NT2 when compared with those from ABA mainly in the seasonal ice region (where mixtures of new ice and first year ice are more prevalent), as shown qualitatively in the color images in Figure 6 and quantitatively in the Figure 11c plots. Figure 10c shows that the mean ice concentrations from NT2 are consistently higher than those from ABA for all seasons except autumn, for which season some years (2002-2004) have practically the same mean ice concentrations from the two algorithms. However, throughout the time series the differences in the ice concentration values are less than 3%, which is within the published errors of the ice concentration algorithms (Comiso et al., 2003). Also, given the differences in the emissivity for the different ice types identified by the different channels, such discrepancies in ice concentration are expected.

Because of the relatively short record length, trend analyses of the AMSR-E data have limited use climatologically, but in this study we calculate trends in the ice cover in order to compare results from the two algorithms. Because of the large seasonality in the ice cover, trend analysis is done using anomalies calculated by subtracting from each data point (in our cause, the monthly average for an individual year) the average for that specific month over each of the years of the record (in our case, 2002-2006). Plots of such anomalies for ice extent, ice area, and ice concentration, using both ABA and NT2 data, are presented in Figure 12, where it is apparent that the two data sets track each other very well. The trends in ice extent are -16.0 ± 1.8 %/decade and -16.4 ± 1.8 %/decade for the ABA and NT2 data, respectively, while the corresponding values for ice area are -16.1 ± 1.9 %/decade and -15.9 ± 2.0 %/decade. The good agreement indicates that despite some disagreements in the derived ice concentrations, the trends derived from the two sets of data are quite close.

Figure 13 presents comparisons of AMSR-E and SSM/I monthly ice extents, areas and ice concentrations, in this case using the Bootstrap algorithm (ABA and SBA) to process data from two different sensors. The mean frequency of the channels in the two sensors are slightly different, and therefore slight differences in sensitivity to atmospheric effects are expected. The main difference, however, is in the resolution, as indicated earlier, which is reflected in the higher values in extents derived from SSM/I data versus from AMSR-E data. The monthly ice areas are closer to each other, while the average ice concentrations are decidedly higher for the AMSR-E data than the SSM/I data. This implies that there are relatively more low ice concentration pixels in the SSM/I data than in the AMSR-E data. This affects the estimates of ice area less because the concentration is low and the net contribution to the ice area is therefore relatively minor.

To evaluate how the trends compare when ice cover is derived from different sensors, the anomalies in ice extents and ice areas as well as ice concentrations are presented in Figure 14. The trends in ice extent calculated from the AMSR-E and SSM/I data sets with the Bootstrap algorithm are shown to be fairly consistent, being -16.0 ± 1.8 %/decade for AMSR-E and -15.8 ± 1.8 %/decade for SSM/I. The corresponding trends in ice area are -16.1 ± 1.9 and 16.7 ± 1.9 %/decade for AMSR-E and SSM/I, respectively. This is encouraging since it indicates that AMSR-E data can be combined with the other historical data to assess the trends of the sea ice cover if biases are taken into consideration.

4. Analysis of Errors

In a few locations and times, there are significant differences in the ice concentrations derived from the AMSR-E data using the ABA and NT2 algorithms. The difference maps in Figures 3-6 indicate that NT2 produces generally higher concentrations than ABA in the marginal ice zone regions in February, May, and November while in the perennial ice region they are on the average compatible. The use of different sets of channels leads to differences in the characterization of ice edges and marginal ice zones, as illustrated in Figure 9, thereby causing differences in the estimates of ice extent. The choice of channels also leads to differences in the perennial ice regions since the emissivity of consolidated ice is spatially more variable with some channels (i.e., 89 GHz channels) than other channels. Nevertheless, there is generally good agreement with the differences typically being no more than about 3%, which is within the estimated errors of the ice concentration algorithms. The differences are minimized mainly because both algorithms make use of the same AMSR-E data to infer the tie-points for consolidated ice and open water (Comiso et al., 2003). Slight adjustments in the tie-points could lead to a closer match in the ice concentration values, but not to identical values throughout, as there are features that one algorithm captures but the other algorithm does not. The cause of these subtle differences may be important to understand in special cases, such as studies of sensible and latent heat polynyas in which quantification of accurate estimates of heat, salinity, and humidity fluxes is desired (Kwok et al., accepted).

Errors in ice extent and area include those associated with the open ocean mask, land/ocean boundary mask, and land mask which are affected only indirectly by the sea ice concentration algorithms. In the Arctic, the uncertainties associated with these parameters can be large because of the presence of extensive ice-free coastlines and many islands, with the latter sometimes so small (compared to the standard grid size of 25 by 25 km) that they are not included as part of the land mass. The land mask is basically fixed, and using a fixed land mask has significant advantages for time series studies. However, as indicated earlier, coastline changes occur due to ice calving, erosion, and other phenomena. An associated question is whether to classify icebergs as part of the sea ice cover or not. The answer is likely no for mass balance studies but yes for many other applications. In the current analysis, icebergs are included in the ice cover calculations, because of failure to identify them properly and to separate them out. The icebergs are not included in full because the emissivity of icebergs is generally lower that that of thick seasonal ice, thereby producing a microwave signature of a partial sea ice cover.

As indicated earlier, the 15% ice edge as inferred from the two algorithms can vary by a few km. This is primarily because of the use of different channels with different resolutions but it can also be because of differences in the location of the tie point for open water. To get an assessment of errors in extent and area associated with errors in the location of the ice edge, we did sensitivity studies using actual data to examine how the ice extent and area change for an error in the ice edge of 6.25, 12.5 and 25 km. Given an ice distribution, we can either add or subtract this value along the ice edge and calculate the resulting change in extent; for the change in area, we assume that the added (or subtracted) data elements all have ice concentrations of 15%. Figure 15 shows the AMSR-E 2005 ice extent and area time series from the ABA algorithm, plus the result of extending the ice edge by 6.25, 12.5, and 25.0 km. Comparing ice extents as depicted in Figure 15 with Figure 10, one can infer that the difference between those of the NT2 and ABA can be explained by errors of about 6.25 km in the ice edge, except during the summer period when other factors must contribute to the difference. With ice area, the variability is similar during the summer but not in the other seasons, when other factors must contribute to the error.

Errors associated with the use of SSM/I data can be evaluated in a similar manner. The biggest source of discrepancies in the SSM/I versus AMSR extents and areas is likely the resolution. The ice edge is better defined with AMSR-E data than with SSM/I data, with the SSM/I ice edges often about 12-25 km equatorward from the AMSR-E ice edge. Comparing the ice extents in Figure 15 and Figure 10, the difference between the AMSR-E and SSM/I results can be explained by a 12.5 km ice-edge error in the winter and autumn and a 25 km ice-edge error in the spring and summer. With ice area, the difference is likely again caused by other factors.

It should also be pointed out that AMSR-E data that are currently being released by the National Snow and Ice Data Center (NSIDC) have been processed using different versions of the algorithms. Different versions are typically minor updates in the tie points to get better consistency with validation data. However, with the ABA algorithm, a significant change was made in the version used for processing Antarctic data in that three channels are now used for the region (instead of only two) as described in Comiso (2004) for consistency with the Arctic algorithm and for improved accuracy. This study made used of ABA data that are derived consistently from 2002 to the present. Similar reprocessing has been planned for the NT2 but has not been implemented. However, only subtle changes in the derived data are expected in the NT2 time series as revealed by the lack of large year-to-year changes in the differences in our analysis.

5. Discussion and Conclusions

The Aqua AMSR-E sensor provides the opportunity to observe the Arctic sea ice cover at a higher resolution and greater spectral range than previously possible and hence an improved accuracy in the characterization of the sea ice cover. The availability of the data is timely in light of rapid changes being observed in parts of the polar regions in recent years and the requirements of more accurate observations. We use ice concentrations derived from two AMSR-E algorithms to assess how consistently the ice cover can be characterized and how estimates of the Arctic sea ice extent and area as well as their trends would be affected by the use of different techniques. Such comparisons are especially important since the extent and area provide the means to assess the state of the sea ice cover and quantify impacts of Arctic warming that may be related to increasing anthropogenic greenhouse gases in the atmosphere. It is also essential to know to what extent such estimates can be algorithm dependent.

The monthly ice concentrations derived from AMSR-E data using the two algorithms differ on average by about 1-3%, with data from near the ice edge generally higher when the NT2 algorithm is used. The standard deviations of the differences are also very small, being ±1.0, ±1.13, ±1.13, and ±1.0 % in summer, autumn, winter and spring, respectively. Slight adjustment in the tie-points for ice and water could make the difference even smaller. It is encouraging to get very good consistency in the extents and areas of the sea ice cover as derived from AMSR-E data using two algorithms that are formulated quite differently and make use of different sets of AMSR-E channels, as it is highly desired that the characterization of the ice cover, including its ice extent and area, would be independent of technique, allowing for confidence in the results.

Likewise, it is satisfying to get good agreement of extents and areas derived when data from AMSR-E are compared with those from SSM/I using the same algorithm. There are slight biases associated with the differences in the resolution of the different sensors in the estimates of ice extents but this is basically negligible in estimates of ice area. A bias, if uncorrected would cause significant errors when combining AMSR-E with historical data. Fortunately, a long overlap of AMSR-E and SSM/I data exists and this will provide the means to remove biases before incorporating the more accurate AMSR-E data in the time series.

The discrepancies in the derived ice concentrations (and also extents and areas) from AMSR-E data using the ABA and NT2 algorithms are likely associated mainly with the choice of channels and in part the choice of tie points. Different channels have different sensitivities to different surfaces. This is especially the case in seasonal regions where new ice is abundant. The use of high frequency channels like the 89 GHz channel, as with NT2, provides the means to identify thin ice; however, the channel is sensitive to atmospheric and surface effects and can produce erroneous ice concentrations if such sensitivity is not properly taken into account. The use of lower frequency channels, as with ABA, provides more contrast between open water and sea ice covered regions and less sensitivity to atmospheric and surface effects but classifies thin ice as having relatively lower concentration than thick ice because of lower emissivity. While this reflects an error in ice concentration (if new ice and thick ice are treated as identical in an ice concentration algorithm), it allows improved ability to assess the widths of the marginal ice zones more accurately and allows the detection of divergence and polynya regions. Overall, the merit of each algorithm depends on application but it is encouraging to know that they produce approximately the same trends in ice extent and area and that the differences in ice concentration values are well within the 5-10% estimated errors in the ice concentration determinations.

Acknowledgements:

The authors grateful appreciate the excellent programming support provided by Robert Gersten and Nick DiGirolamo of Adnet Inc. The project was funded by the Crospheric Sciences Program at NASA Headquarters.

References:

Bjorgo, E. , O.M. Johannessen, and M.W. Miles, "Analysis of merged SSMR-SSM/I time series of Arctic and Antarctic sea ice parameters 1978-1995," *Geophys. Res. Lett.*, *24*, 413-416, 1997.

Cavalieri, D.J., P. Gloersen, W.J. Campbell, Determination of sea ice parameters with the Nimbus7 SMMR, *J. Geophys Res.*, *89*, 5355-5369, 1984.

Cavalieri, D.J., P. Gloersen, C. Parkinson, J. Comiso, and H.J. Zwally, Observed hemispheric asymmetry in global sea ice changes, *Science, 278*(7), 1104-1106,1997.

Cho, K., N. Sasaki, H. Shimoda, T. Sakata and F. Nishio, Evaluation and improvement of SSM/I sea ice concentration algorithms for the Sea of Okhotsk, *J. Remote Sensing of Japan,* **16**(2), 47-58, 1996.

Comiso, J. C., Sea ice microwave emissivities from satellite passive microwave and infrared observations, *J. Geophys. Res., 88*(C12), 7686-7704, 1983.

Comiso, J. C., A rapidly declining Arctic perennial ice cover, *Geophys Res. Letts., 29(20), 1956, doi:10.1029/2002GL015650,* 2002.

Comiso, J.C., Sea ice algorithm for AMSR-E, *Rivista Italiana di Telerilevamento (Italian Journal of Remote Sensing), 30/31*, 119-130, 2004.

Comiso, J.C., and R. Kwok, The summer Arctic sea ice cover from satellite observations, *J. Geophys. Res., 101*(C2), 28397-28416, 1996.

Comiso, J. C. and C. L. Parkinson, Satellite observed changes in the Arctic, *Phys. Today 57*(8), 38-44, 2004.

Comiso, J.C., and K. Steffen, Studies of Antarctic sea ice concentrations from satellite data and their applications, *J. Geophys. Res., 106*(C12), 31361-31385, 2001.

Comiso, J. C., D. J. Cavalieri, and T. Markus, Sea ice concentration, ice temperature, and snow depth, using AMSR-E data, *IEEE TGRS, 41(2),* 243-252, 2003.

Comiso, J.C., D. Cavalieri, C. Parkinson, and P. Gloersen, Passive microwave algorithms for sea ice concentrations, *Remote Sensing of the Env., 60*(3), 357-384, 1997.

Gloersen P., W. Campbell, D. Cavalieri, J. Comiso, C. Parkinson, H.J. Zwally, Arctic and Antarctic Sea Ice, 1978-1987: Satellite Passive Microwave Observations and Analysis, *NASA Spec. Publ. 511*, 1992.

Grenfell, T.C. 1992.Surface-based passive microwave studies of multiyear ice. *J. Geophys. Res.,* **97**(C3), 3485-3501.

Holland, M. M., C.M. Bitz, Polar amplification of climate change in the Coupled Model Intercomparison Project, *Clim. Dyn. 21*, 221-232, 2003.

Kwok, R., J. C. Comiso, S. Marin, and R. Drucker, Ross Sea polynyas: Response of ice concentration retrievals to large areas of thin ice, *J. Geophys. Res.,* (In press).

Markus, T. and D.J. Cavalieri, An enhancement of the NASA team sea ice algorithm, *IEEE Trans. Geosci. Remote Sensing,* 38, 1387-1398, 2000.

Markus, T. and S.T. Dokken, Evaluation of Arctic late summer passive microwave sea ice retrievals, *IEEE Trans. Geosci. Remote Sensing*, 40, 348-356, 2002.

Matzler, C., R. O. Ramseier, and E. Svendsen, "Polarization effects in sea ice signatures," *IEEE J. Oceanic Engineering*, Vol. OE-9, pp. 333-338, 1984.

Parkinson, C.L., and J.C. Comiso, Antarctic Sea Ice Parameters from AMSR-E using two techniques and comparison with Sea Ice from SSM/I, J. Geophys. Res. (submitted, 2007)

Parkinson, C.L., D.J Cavalieri, P. Gloersen, H.J. Zwally, and J.C. Comiso, Arctic sea ice extents, areas, and trends, 1978-1996, *J. Geophys. Res.*, *104*(C9), 20837-20856, 1999.

Parkinson, C. L., J. C. Comiso, H. J. Zwally, D. J. Cavalieri, P. Gloersen, and W. J. Campbell, Arctic Sea Ice 1973-1976 from Satellite Passive Microwave Observations, *NASA Spec. Publ. 489*, 1987.

Steffen, K., D. J. Cavalieri, J. C. Comiso, K. St. Germain, P. Gloersen, J. Key, and I. Rubinstein, "The estimation of geophysical parameters using Passive Microwave Algorithms," Chapter 10, *Microwave Remote Sensing of Sea Ice,* (ed. by Frank Carsey), American Geophysical Union, Washington, D.C., 201-231, 1992.

Svendsen, E., C. Matzler, T.C. Grenfell, "A model for retrieving total sea ice concentration from a spaceborne dual-plarized passive microwave instrument operating near 90 GHz," *Int. J. Rem. Sens.*, Vol. 8, pp. 1479-1487, 1987.

Swift, C.T., L.S. Fedor, and R.O. Ramseier, An algorithm to measure sea ice concentration with microwave radiometers, *J. Geophys. Res.*, 90(C1), 1087-1099, 1985.

Vant, M.R., R.B. Gray, R.O. Ramseier, and V. Makios. 1974. Dielectric properties of fresh and sea ice at 10 and 35 GHz, *J. Applied Physics*, *45*(11), 4712-4717.

Walsh, J.E., and C.M. Johnson, An analysis of Arctic sea ice fluctuations, *J. Phys. Ocean., 9,* 580-591, 1979.

Figures Legends

Figure 1. Location map of the Arctic showing various regions of interest and climatological sea ice cover at the seasonal times of ice minimum and maximum.

Figure 2. Scatter plots of brightness temperatures illustrating the distribution of open ocean area and the masking procedure using 19 GHz vertically polarized data (V19) versus the difference between 22 GHz or 23 GHZ vertically polarized data (V22 or V23, respectively) and 19 GHz or 18 GHz vertically polarized data (V19 or V18, respectively) from (a) SSM/I and (b) AMSR-E, and V19 or V18 data versus 37 GHz or 36 GHz vertically polarized data (V37 or V36, respectively) from (c) SSM/I and (d) AMSR-E. The mask for SMMR is similar to that in (c) and (d) but has greater separation because SMMR has an 18 GHz channel (which is less subject to weather effects) instead of 19 GHz.

Figure 3. Scatter plots of gradient and polarization ratios illustrating the distribution of open ocean area using gradient ratio of V19 and V37 versus polarization ration of H19 and V19 from (a) SSM/I and (b) AMSR-E data and also gradient ratio of V19 and V22 versus polarization ratio of H19 and V19 from (c) SSM/I and (d) AMSR-E data.

Figure 4. Color-coded monthly ice concentration maps derived from AMSR-E data for August 2002, 2003, 2004 and 2005 using the ABA and NT2 algorithms, and the corresponding difference maps.

Figure 5. Same as Figure 3 except for November.

Figure 6. Same as Figure 3 except for February and for the years 2003-2006 rather than 2002-2005.

Figure 7. Same as Figure 5 except for May.

Figure 8. Histograms of differences in ice concentration (in percentage) between ABA and NT2.

Figure 9. Ice concentration values along a transect from open water to the ice pack at (a) 35°E and (b) 45°E in the Barents Sea on february 19, 2006, as derived from AMSR-E data using the ABA and NT2 algorithms and AMSR-E data .

Figure 10. Comparison of daily (a) ice extent and (b) ice area using the ABA and NT2 algorithms on AMSR-E data and the SBA algorithm on SSM/I data in 2005.

Figure 11. Plots of monthly values of (a) ice extent; (b) ice area; and (c) ice concentration from June 2002 through November 2006 derived from AMSR-E data using the ABA and NT2 algorithms. Each monthly ice concentration data point is the average of the daily ice concentration averages during the month.

Figure 12. Plots of anomalies of the monthly values of (a) ice extent; (b) ice area; and (c) ice concentration from June 2002 through November 2006 derived from AMSR-E data using the ABA and NT2 algorithms.

Figure 13. Plots of monthly values of (a) ice extent; (b) ice area; and (c) ice concentration from June 2002 through November 2006 derived from the AMSR-E and SSM/I data using the ABA algorithm. Each monthly ice concentration data point is the average of the daily ice concentration averages during the month.

Figure 14. Plots of the anomalies of the monthly values of (a) ice extent; (b) ice area; and (c) ice concentration from June 2002 through November 2006 derived from the AMSR-E and SSM/I data using the Bootstrap algorithm (ABA and SBA).

Figure 15. (a) Sensitivity plot of the seasonal cycle of monthly average ice extent, with the

baseline curve being the AMSR-E extent and the additional curves being the extents derived if the ice edge is further south by 6.25 km, 12.5 km, and 25 km. (b) Sensitivity plot similar to (a) but using monthly average ice area.

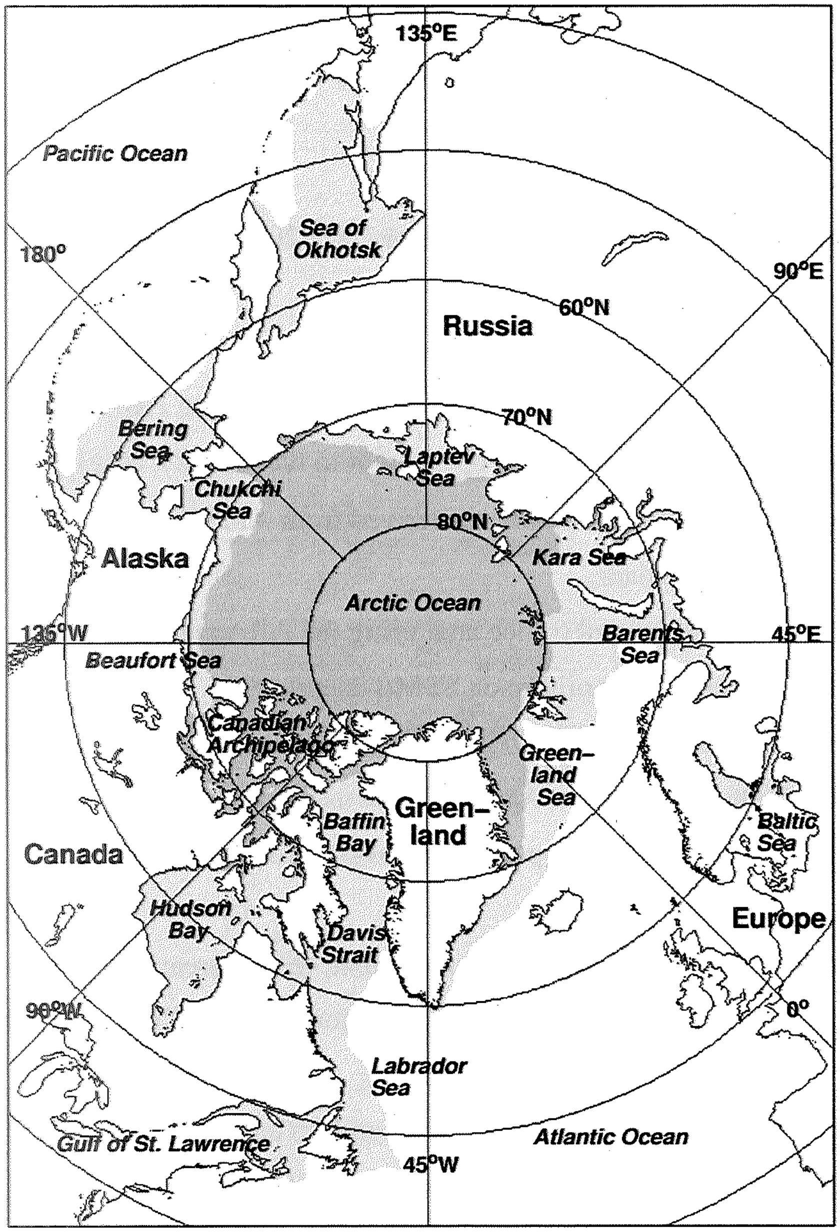

Figure 1. Location map of the Arctic showing various regions of interest and climatological sea ice cover at the seasonal times of ice minimum and maximum. concentration averages during the month.

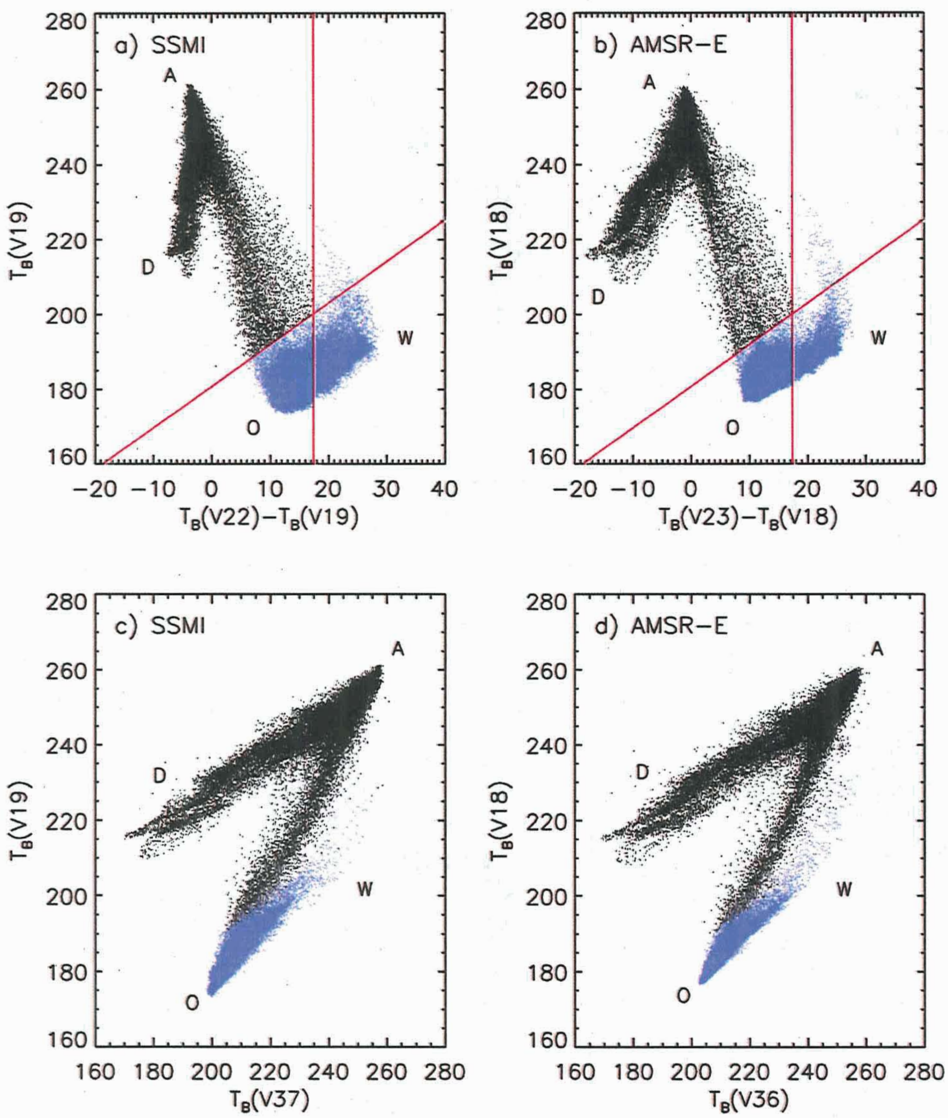

Figure 2. Scatter plots of brightness temperatures illustrating the distribution of open ocean area (blue dots) and the masking procedure using 19 GHz vertically polarized data (V19) versus the difference between 22 GHz or 23 GHZ vertically polarized data (V22 or V23, respectively) and 19 GHz or 18 GHz vertically polarized data (V19 or V18, respectively) from (a) SSM/I and (b) AMSR-E, and V19 or V18 data versus 37 GHz or 36 GHz vertically polarized data (V37 or V36, respectively) from (c) SSM/I and (d) AMSR-E. The mask for SMMR is similar to that in (c) and (d) but has greater separation because SMMR has an 18 GHz channel (which is less subject to weather effects) instead of 19 GHz.

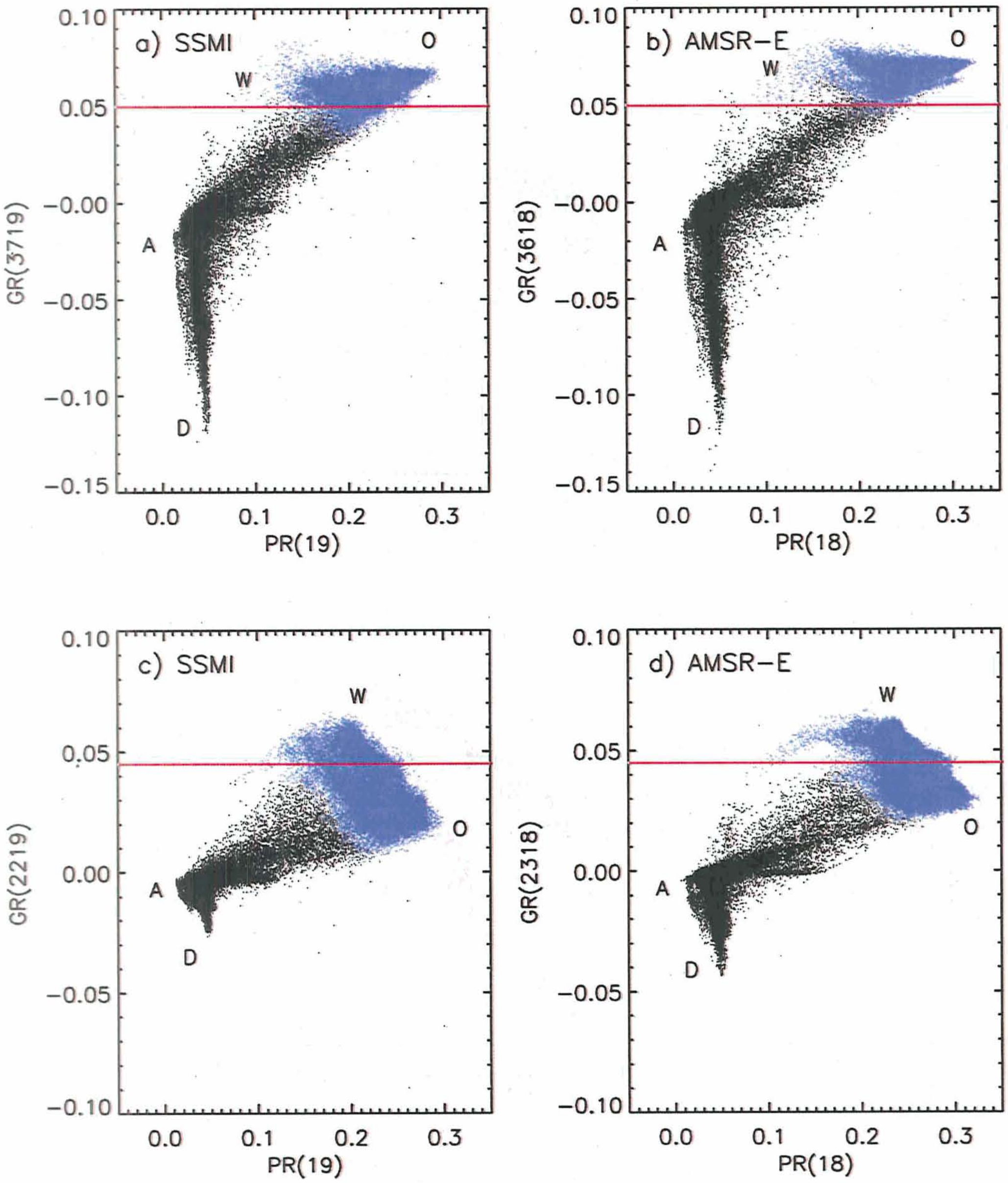

Figure 3. Scatter plots of gradient and polarization ratios illustrating the distribution of open ocean area (in blue) using gradient ratio of V19 and V37 versus polarization ration of H19 and V19 from (a) SSM/I and (b) AMSR-E data and also gradient ratio of V19 and V22 versus polarization ratio of H19 and V19 from (c) SSM/I and (d) AMSR-E data.

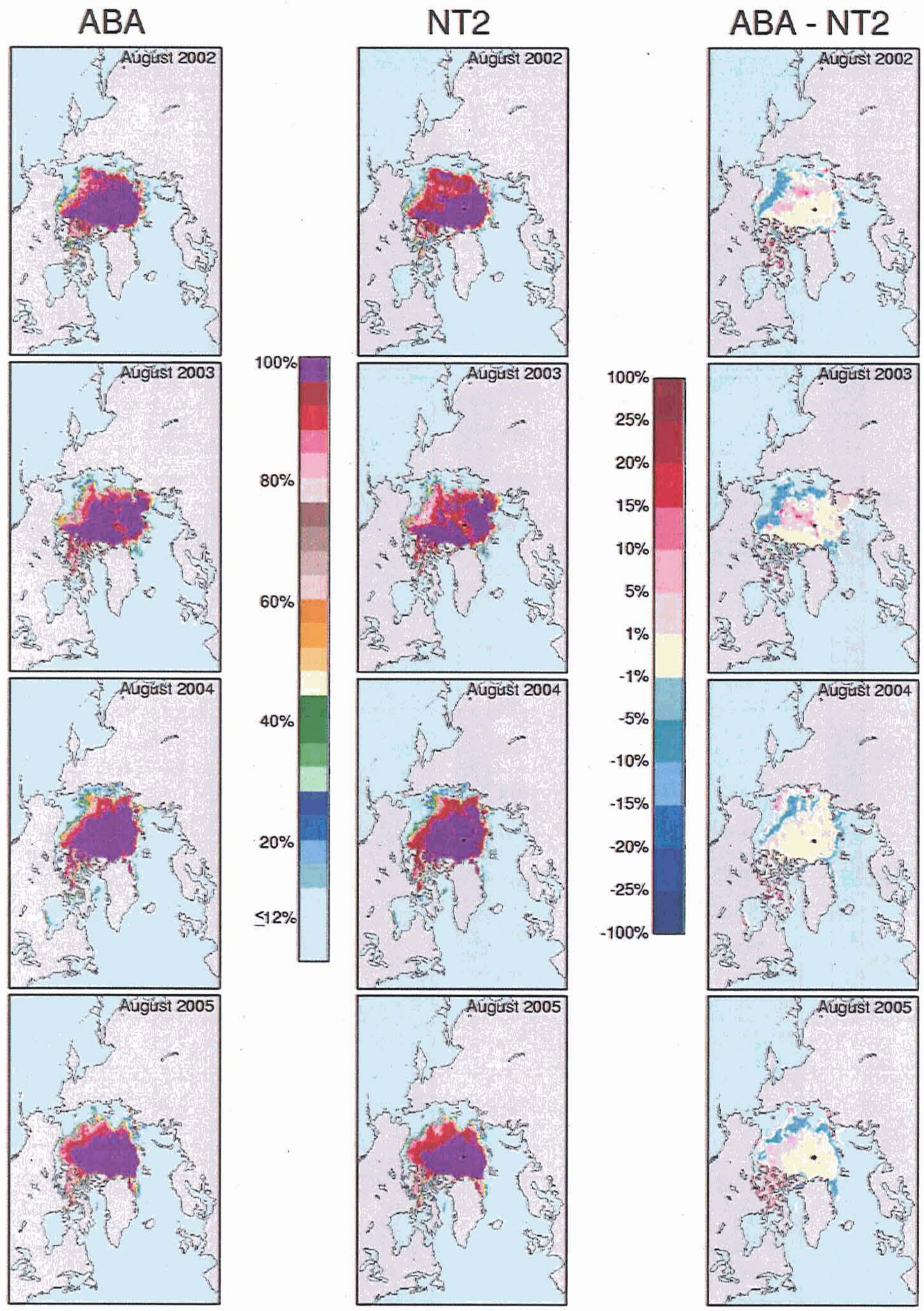

Figure 4. Color-coded monthly ice concentration maps derived from AMSR-E data for August 2002, 2003, 2004 and 2005 using the ABA and NT2 algorithms, and the corresponding difference maps.

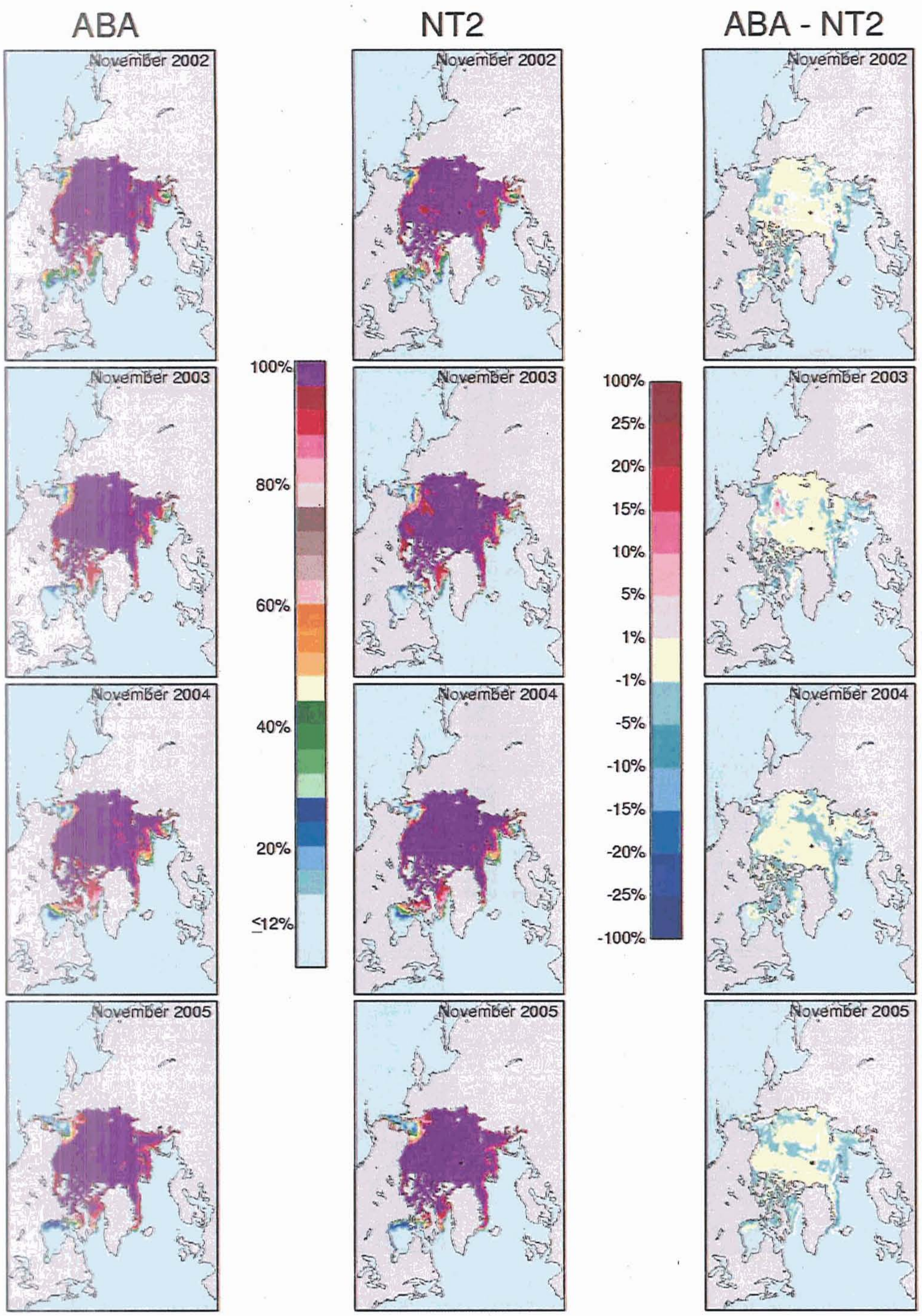

Figure 5. Same as Figure 4 except for November.

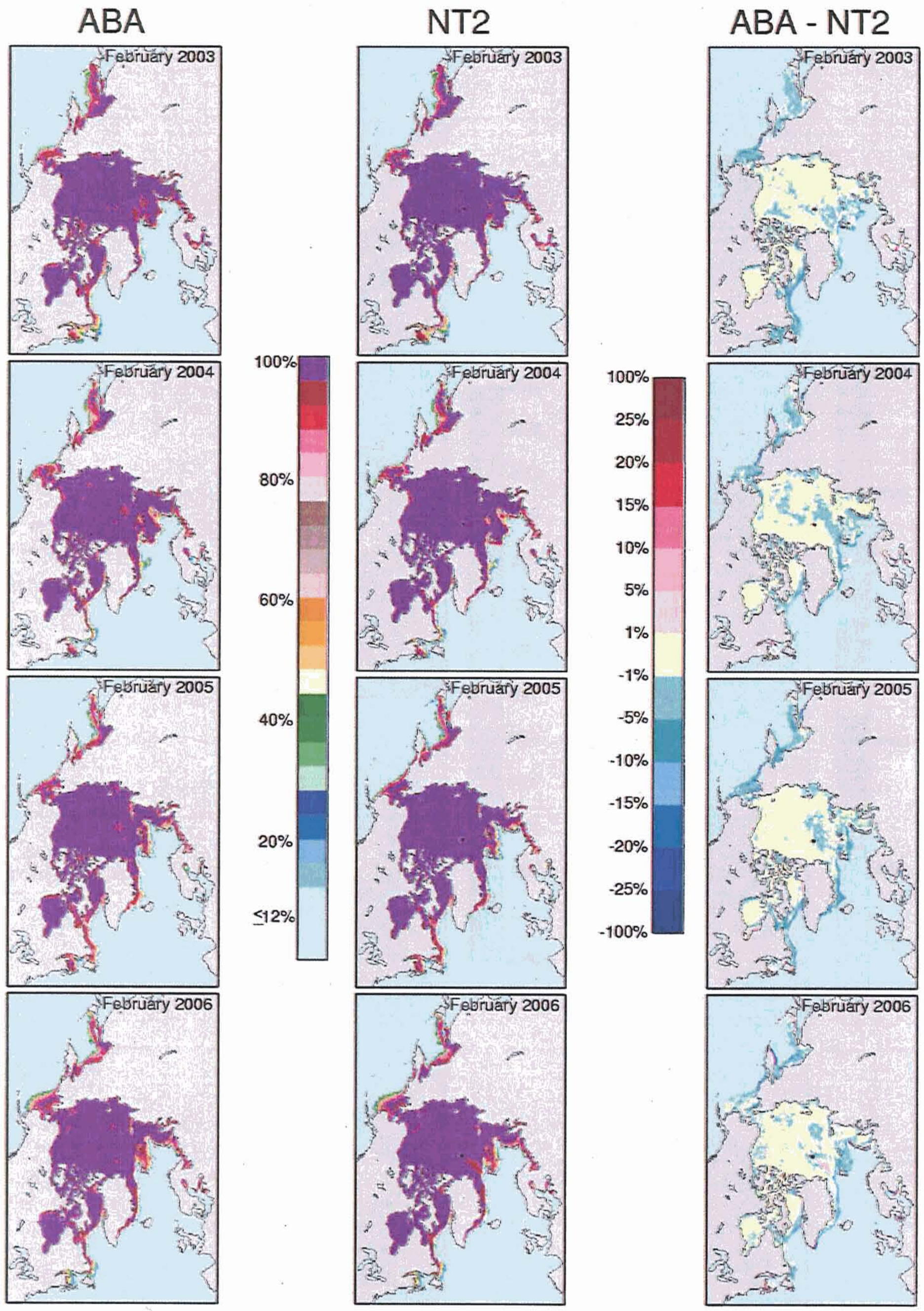

702 Figure 6. Same as Figure 4 except for February and for the years 2003-2006 rather than 2002-
703 2005.

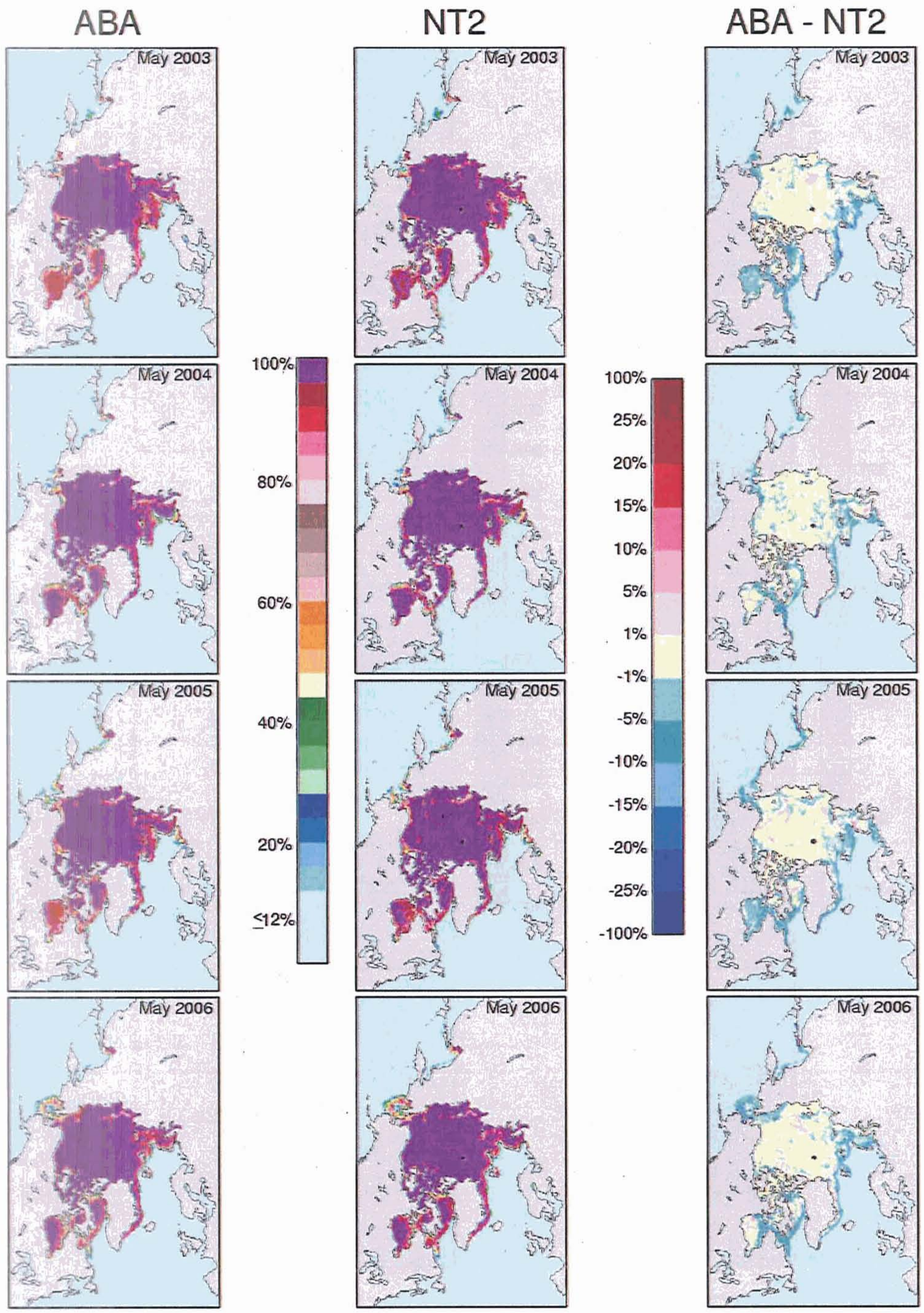

Figure 7. Same as Figure 4 except for May.

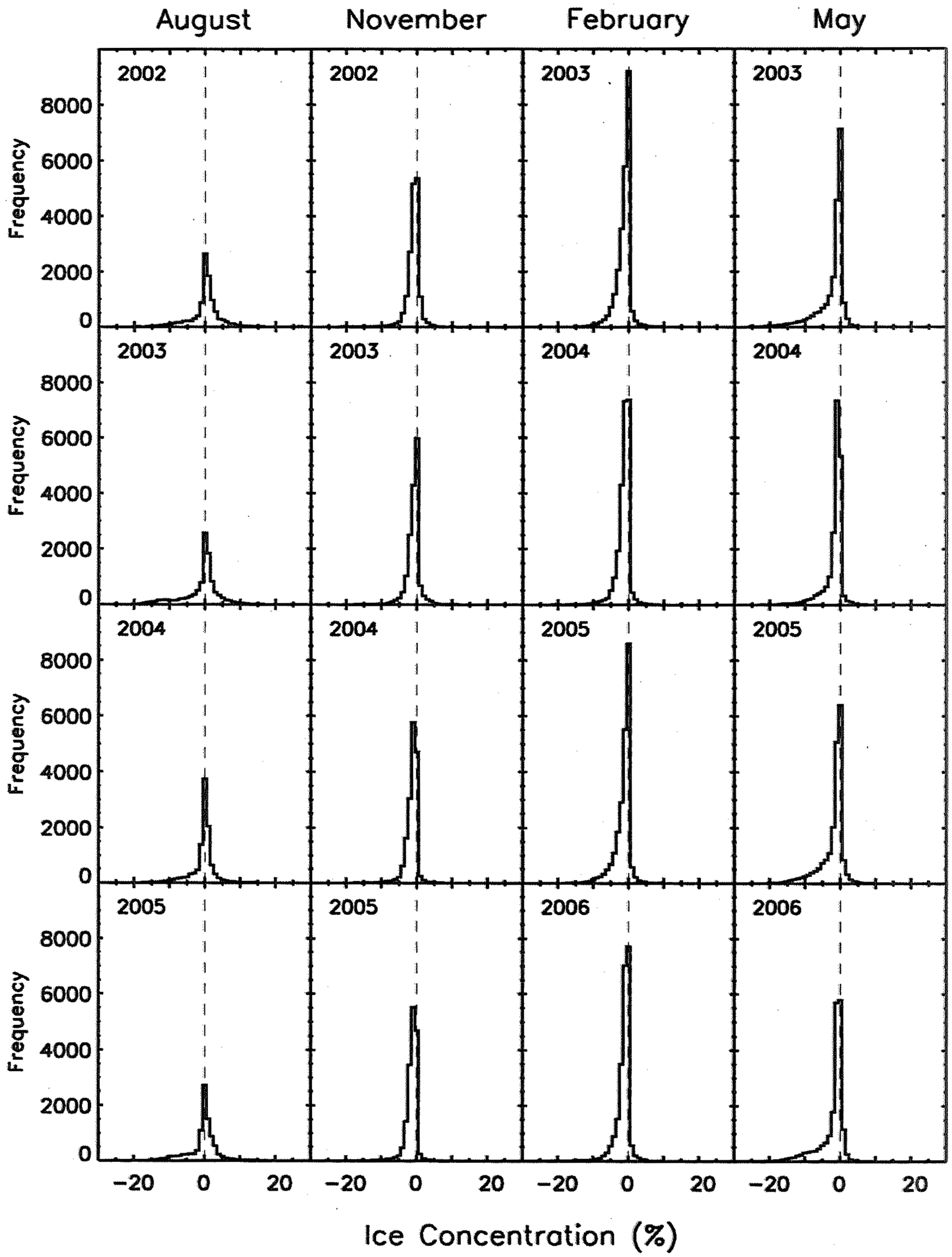

Figure 8. Histograms of differences in ice concentration (in percentage) between ABA and NT2.

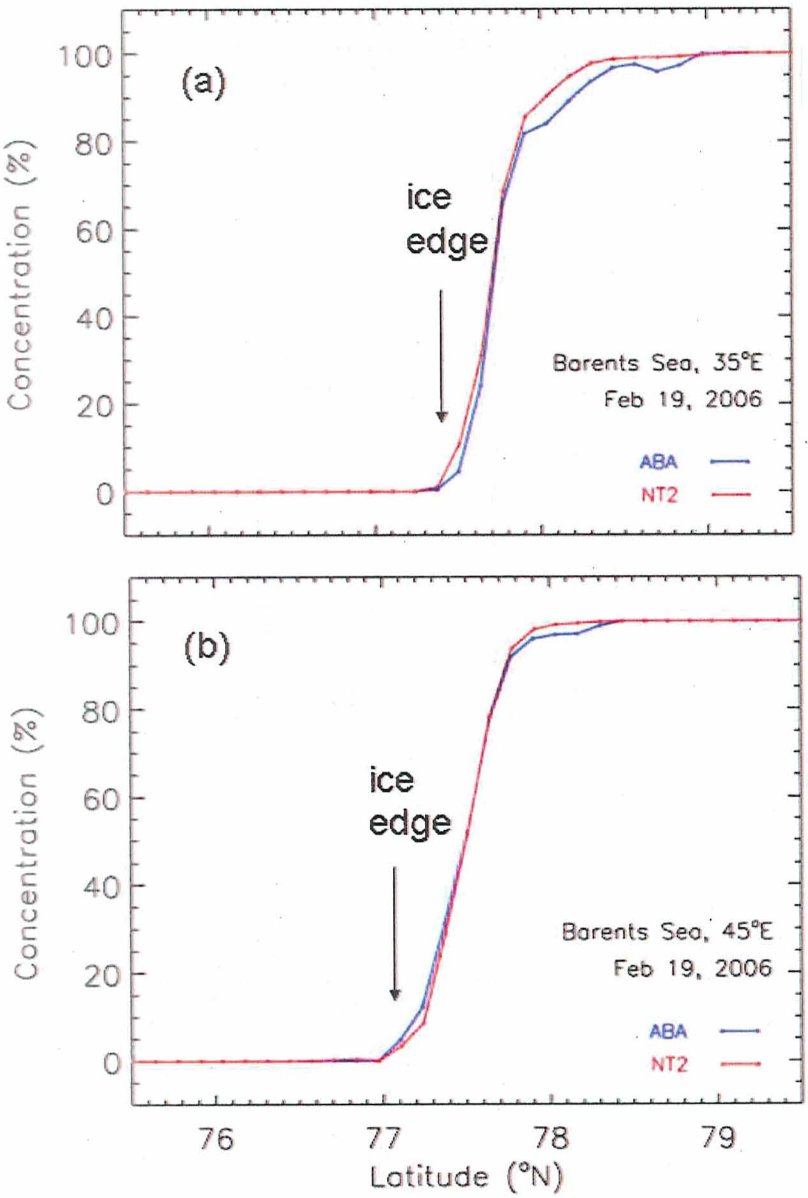

Figure 9. Ice concentration values along a transect from open water to the ice pack at (a) 35°E and (b) 45°E in the Barents Sea on february 19, 2006, as derived from AMSR-E data using the ABA and NT2 algorithms and AMSR-E data .

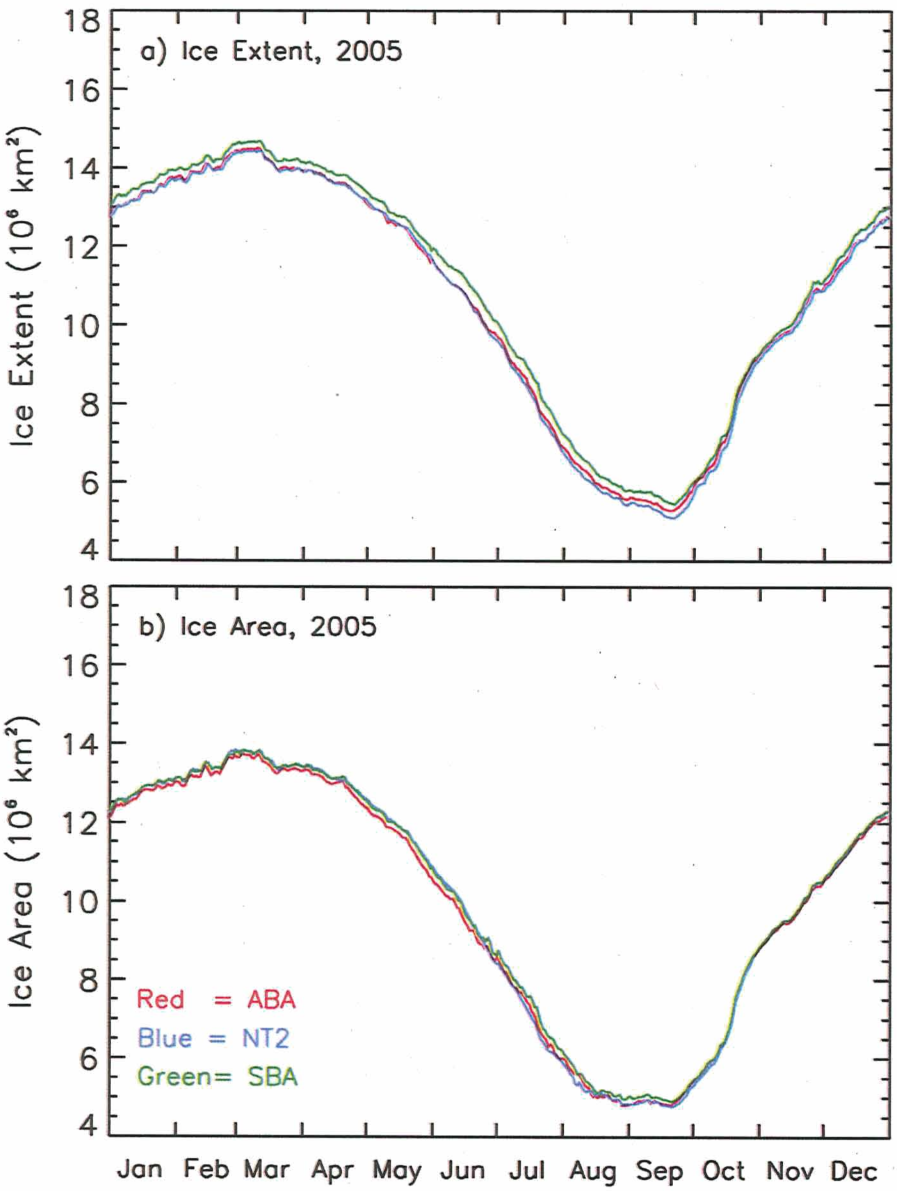

Figure 10. Comparison of daily (a) ice extent and (b) ice area using the ABA and NT2 algorithms on AMSR-E data and the SBA algorithm on SSM/I data in 2005.

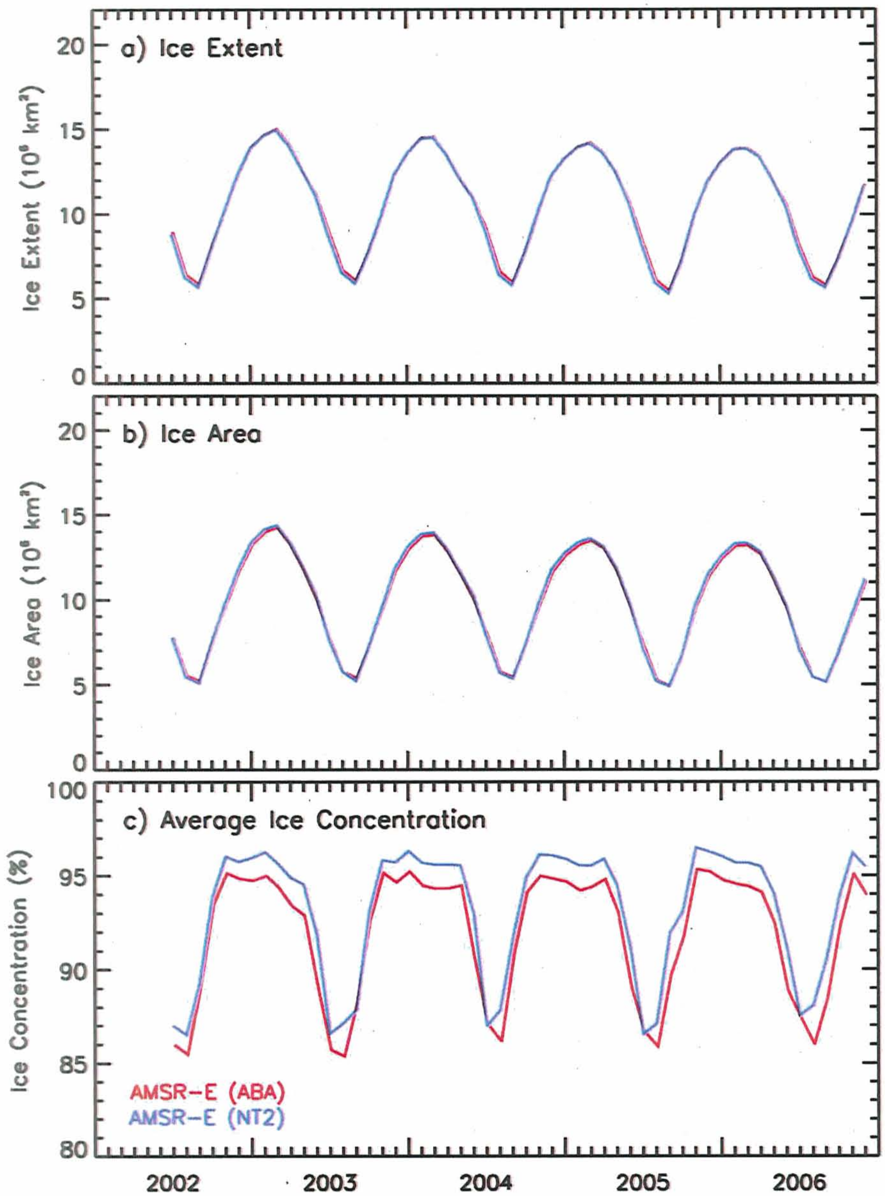

Figure 11. Plots of monthly values of (a) ice extent; (b) ice area; and (c) ice concentration from June 2002 through November 2006 derived from AMSR-E data using the ABA and NT2 algorithms. Each monthly ice concentration data point is the average of the daily ice

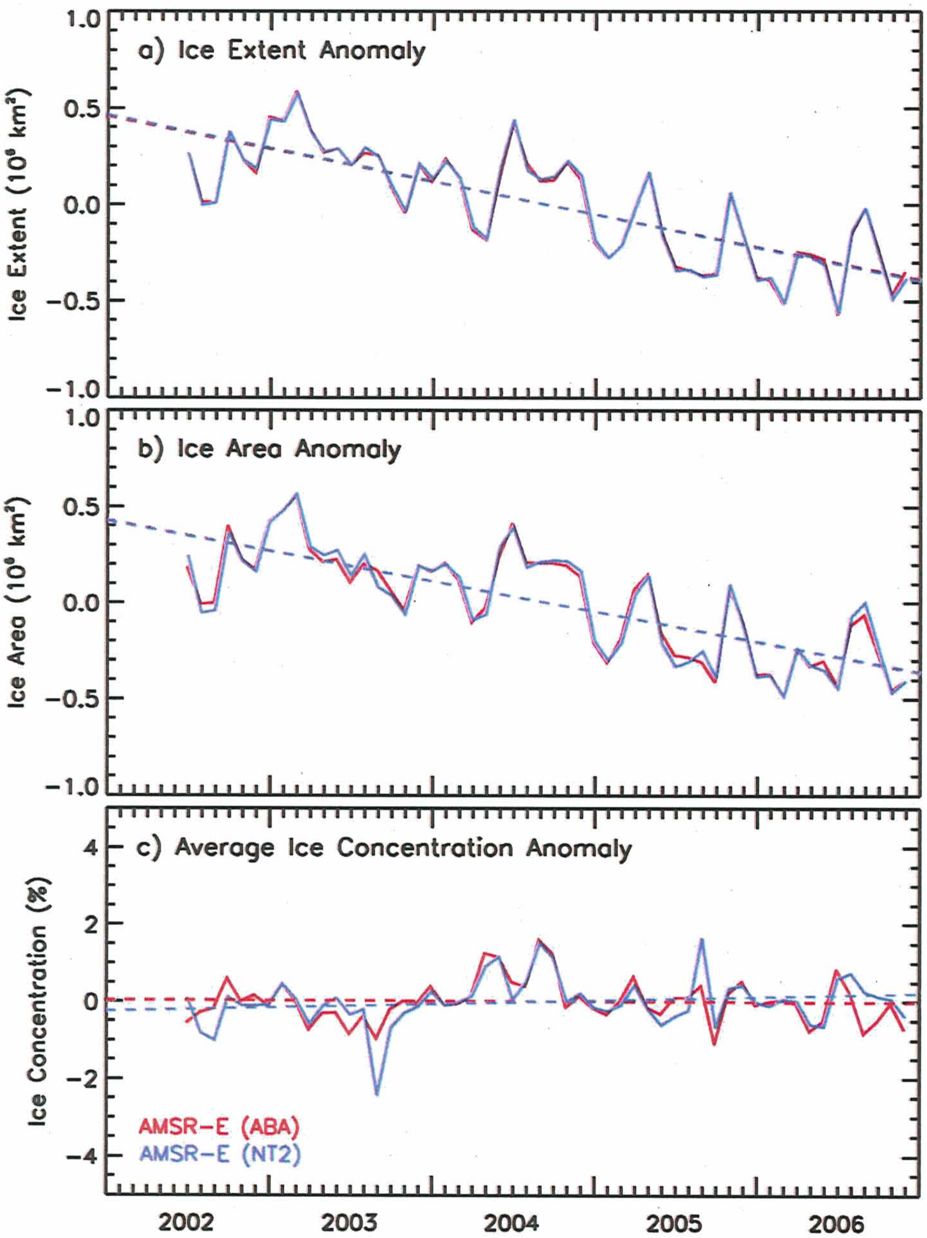

Figure 12. Plots of anomalies of the monthly values of (a) ice extent; (b) ice area; and (c) ice concentration from June 2002 through November 2006 derived from AMSR-E data using the ABA and NT2 algorithms.

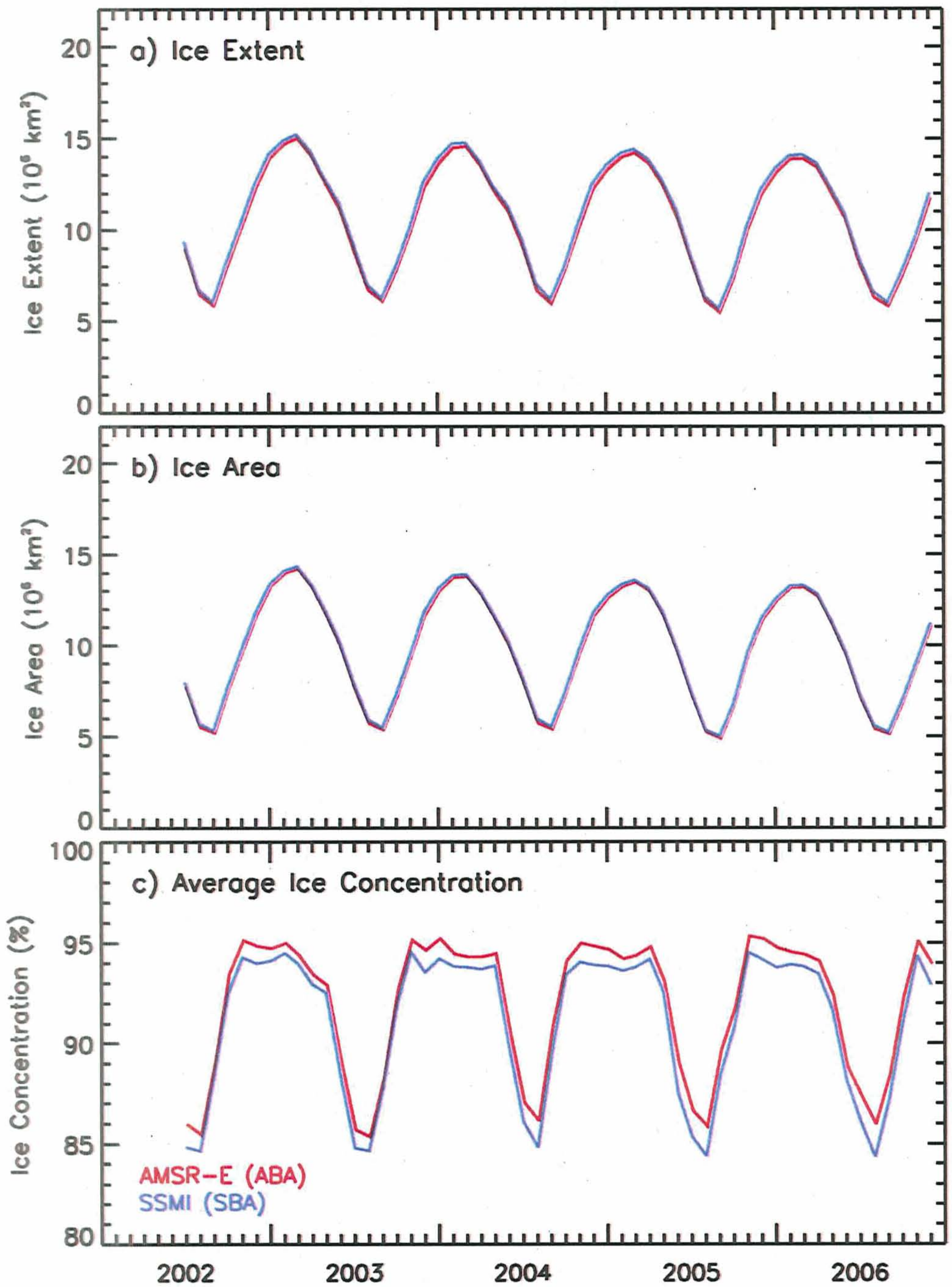

Figure 13. Plots of monthly values of (a) ice extent; (b) ice area; and (c) ice concentration from June 2002 through November 2006 derived from the AMSR-E and SSM/I data using the ABA algorithm. Each monthly ice concentration data point is the average of the daily ice concentration averages during the month.

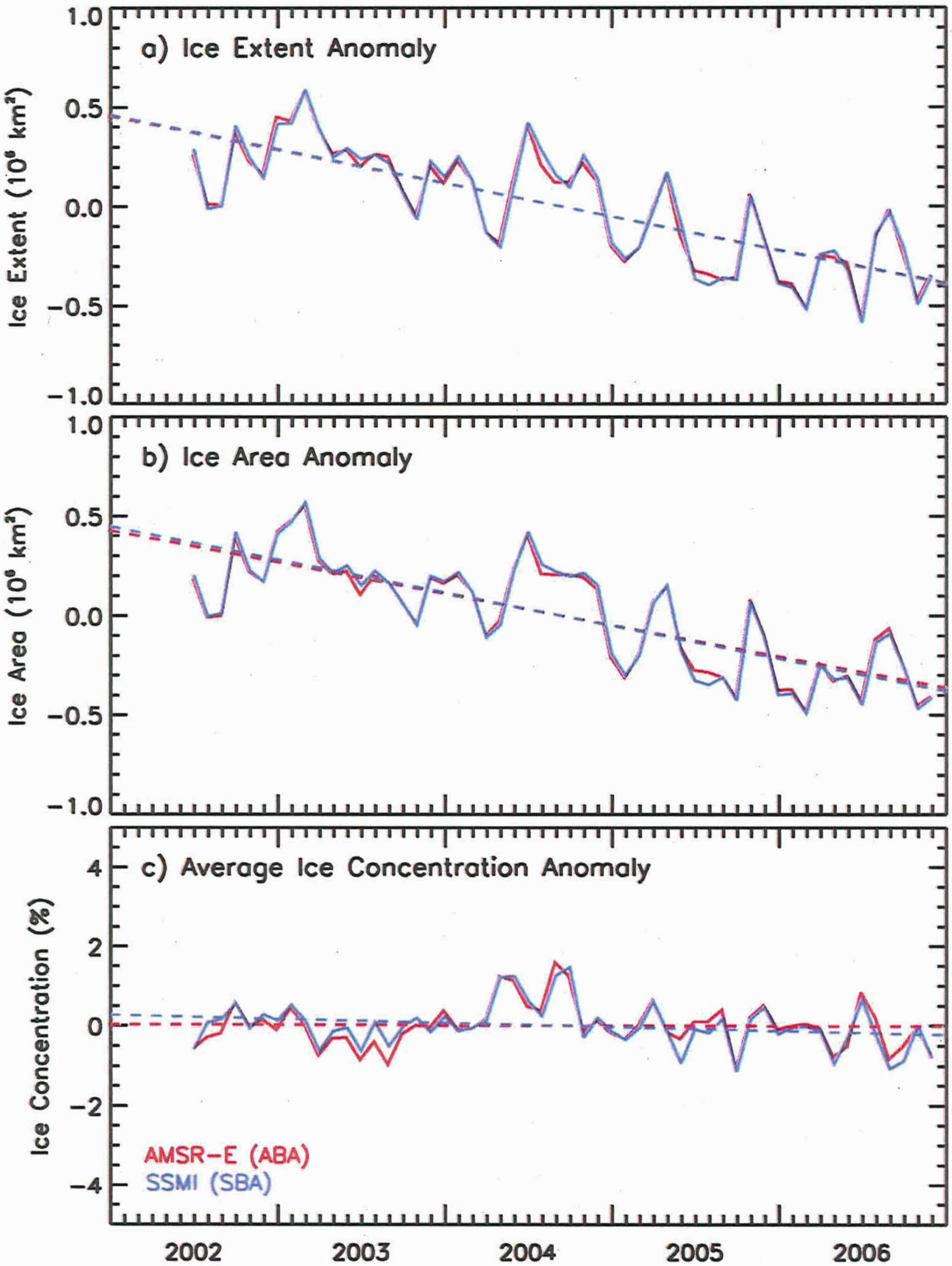

Figure 14. Plots of the anomalies of the monthly values of (a) ice extent; (b) ice area; and (c) ice concentration from June 2002 through November 2006 derived from the AMSR-E and SSM/I data using the Bootstrap algorithm (ABA and SBA).

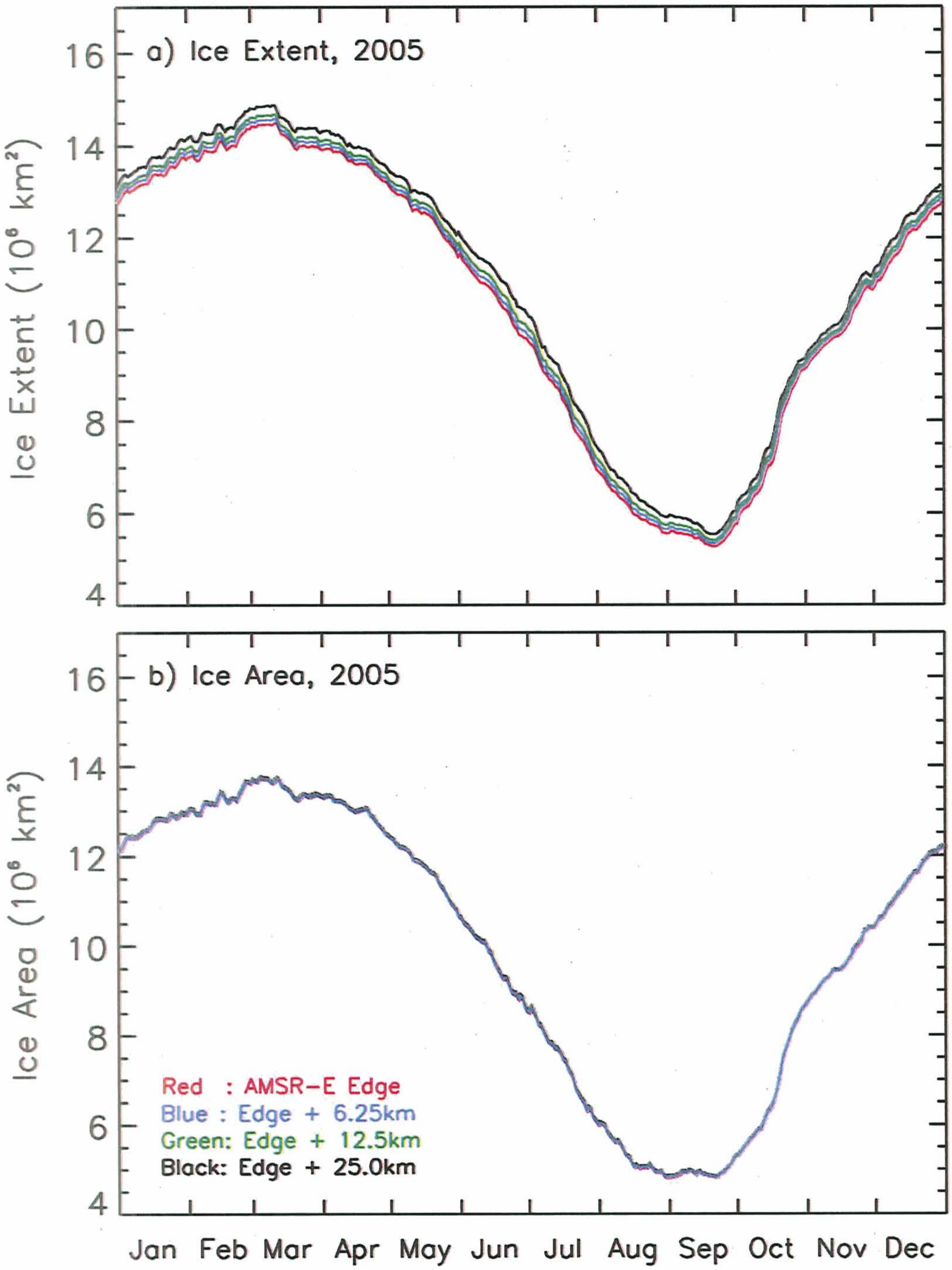

Figure 15. (a) Sensitivity plot of the seasonal cycle of monthly average ice extent, with the baseline curve being the AMSR-E extent and the additional curves being the extents derived if the ice edge is further south by 6.25 km, 12.5 km, and 25 km. (b) Sensitivity plot similar to (a) but using monthly average ice area.